To the Graduate Council:

I am submitting herewith a dissertation written by David Howard Huddleston entitled "Aerodynamic Design Optimization Using Computational Fluid Dynamics." I have examined the final copy of this dissertation for form and content and recommend that it be accepted in partial fulfillment of the requirements for the degree of Doctor of Philosophy, with a major in Engineering Science.

John E. Caruthers

John E. Caruthers, Major Professor

We have read this dissertation and recommend its acceptance:

C. Wayne Mastin

Roy J. Schulz

John Steinhoff

Accepted for the Council:

Vice Provost
and Dean of The Graduate School

AERODYNAMIC DESIGN OPTIMIZATION USING COMPUTATIONAL FLUID DYNAMICS

A Dissertation

Presented for the

Doctor of Philosophy

Degree

The University of Tennessee, Knoxville

David Howard Huddleston

December 1989

ACKNOWLEDGMENTS

The research reported herein was sponsored by the Arnold Engineering Development Center (AEDC), Air Force Systems Command, Arnold Air Force Base, Tennessee, under Contract No. F40600-85-C0026. Sincere appreciation is extended to the United States Air Force and to Sverdrup Technology, Inc., contract operator for aeropropulsion testing at the AEDC, for the opportunity to participate in this research.

In preparing this dissertation, many individuals provided generous assistance without which successful completion of the research would have been impossible. Since it is not practical to acknowledge each individual, the author expresses his gratitude collectively to the members of his graduate committee and to the members of the Propulsion Computational Technology Section of Sverdrup Technology, Inc.

During graduate study and preparation of this dissertation, many sacrifices were made by the author's immediate family. It would have been impossible to complete the graduate program were it not for the patience and understanding exhibited by the author's wife and children during the periods when "Daddy" was unavailable. The greatest debt of gratitude is owed to the author's parents, Porter Howard and Billie Love Huddleston, for providing an environment that instilled the author's desire to attain a

higher education and for the many sacrifices made to assure that the opportunity to attain a higher education was available to the author. In recognition of their love and sacrifice, this dissertation is dedicated to the author's parents.

ABSTRACT

An aerodynamic design optimization technique is presented that couples direct optimization algorithms with the analysis capability provided by appropriate computational fluid dynamics (CFD) programs. This technique is intended to be an aid in designing the aerodynamic shapes and establishing test conditions required for the successful simulation of aircraft engine inlet conditions in a ground test environment. However, the method is also applicable to other aerodynamic design problems such as airfoil design, turbomachinery cascade design, and nozzle design.

The approach involves minimization of a nonlinear least-squares objective function which may be defined in a region remote to the geometric surface being optimized. In this study, finite-difference Euler and Navier-Stokes codes were applied to obtain the objective function evaluations, although the applied optimization method can be coupled with any appropriate CFD analysis technique. Using CFD to compute design space gradients within an optimization algorithm has received little prior attention in the literature. It is demonstrated, herein, that CFD can be used in this manner by applying the developed design technique to a variety of aerodynamic design problems. Results are presented for several typical aerospace examples, including algebraic test functions, inviscid and

viscous flow over airfoils, flows in convergent/divergent nozzles in both two and three dimensions, and supersonic flow about a planar forebody simulator.

TABLE OF CONTENTS

PAGE

LIST OF TABLES

LIST OF FIGURES

FIGURE | Page

FIGURE		Page

FIGURE Page

NOMENCLATURE

B	Jacobian approximation
C_1	first algebraic test function convergence criterion--see Table 1
C_2	second algebraic test function convergence criterion--see Table 1
F	least-squares objective function
$g_i^p(u)$	Bernstein basis function defined by Eq. (3.3.3)
J	Jacobian matrix of $\underline{R}$ with respect to $\underline{P}$ defined by Eq. (3.2.4)
M	total number of design parameters
M_x	Mach number component along the x-axis
M_y	Mach number component along the y-axis
M_z	Mach number component along the z-axis
N	total number of residual components
N_r	number of reference plane points
N_c	number of parameter constraints
$\underline{P}$	design parameter vector
P_i	individual design parameter
P_T	total pressure
r_i	least-squares residual component
$\underline{R}$	residual component vector
RP	aerodynamic optimization reference plane
t	NACA0012 airfoil thickness parameter--see Eq. (4.2.1)
T_T	total temperature
u	Bernstein-Bezier interpolation parameter--see Eqs. (3.3.1) and (3.3.2)

v	Bernstein-Bezier interpolation parameter--see Eq. (3.3.2)
w	Bernstein-Bezier interpolation parameter--see Eq. (3.3.2)
x	NACA0012 airfoil axial coordinate--see Eq. (4.2.1)
$\underline{x}_i$	position vectors of Bezier control points--see Eq. (3.3.1)
$\underline{x}_{ijk}$	position vectors of three-dimensional Bezier control points--see Eq. (3.3.2)
$\underline{x}(u)$	Bernstein-Bezier polynomial--see Eq. (3.3.1)
$\underline{x}(u,v,w)$	three-dimensional Bezier polynomial--see Eq. (3.3.2)
$y(x)$	function used to define NACA0012 airfoil--see Eq. (4.2.1)
$\Delta\underline{P}$	computed change in design parameter vector
ϕ_i	imposed barrier functions

1.0 INTRODUCTION

During the past three decades, Computational Fluid Dynamics (CFD) has emerged as a discipline that allows the analysis of many previously intractable problems in fluid mechanics. Although CFD is still in a stage of rapid growth and development, it is already being widely used to enhance the aerodynamic design process [1][1]. The most common application of CFD in aerodynamic design has been to provide direct analyses of existing or proposed design configurations as a means of evaluating the design quality. Coupling numerical optimization methods with the versatile analysis capability afforded by modern CFD techniques offers the potential to allow many aerodynamic designs to be optimized relative to specified design criteria in a fashion heretofore impossible.

The objective of this dissertation is to present a design optimization method that has been developed for application to complex aerodynamic design problems. This is accomplished by optimizing selected design parameters through the minimization of a nonlinear least-squares objective function. Flexibility in the type of designs that can be considered is provided by using the powerful analysis capability afforded by modern CFD codes to produce the function evaluations required by the optimization algorithm.

---

1 Numbers in brackets refer to similarly numbered references in the bibliography.

This direct optimization approach is applicable in both two and three dimensions and, in principle, any CFD technique appropriate to the flow regime of interest could be used.

Using CFD to compute design space gradients within an optimization algorithm has received little prior attention in the literature. It is demonstrated, herein, that Euler or Navier-Stokes CFD simulations are reliable enough to be used in this manner by applying the developed design technique to a variety of aerodynamic design problems. The test problems were constructed to illustrate that this approach can be applied to realistic designs by deliberately selecting poor initial conditions for the optimization algorithm.

The aerodynamic design optimization problem which motivated this research is illustrated in Figure 1[2]. This figure depicts a free-jet inlet-engine test configuration within a generic ground test facility designed to evaluate the performance of an integrated propulsion system. The design requirement is to produce a flow field across a specified inlet reference plane in the free-jet installation that is similar, within a predefined tolerance, to that which would be encountered in flight [2]. One proposed way of achieving this is by appropriately designing a portion of geometry within the test configuration, hereafter referred

---

2 All figures may be found in Appendix A.

to as the forebody simulator, and/or varying free-jet flow conditions (total pressure, total temperature, flow angle, and Mach number) to produce the desired flow field at the inlet reference plane [2]. The plane where fluid dynamic variables are specified will hereafter be referred to as the reference plane (RP). The fundamental assumption of this free-jet test concept is that adequate similitude is attained whenever the fluid dynamic state at the indicated reference plane adequately matches that which is specified for a given operating condition.

The task of designing such a "flow tailoring" geometry and the corresponding test conditions is formidable. The test designer must specify a forebody simulator geometry and free-jet fluid properties that produce, within design tolerance, the desired fluid dynamic state at the region of interest. Current forebody simulator design methods rely heavily upon prior experience to guide a trial-and-error design approach utilizing subscale testing and CFD analyses to evaluate the candidate designs. This process is inefficient, does not ensure an orderly progression toward an acceptable design, and does not ensure that the final design is optimum. Thus, the specific purpose of the research reported herein was to develop a reliable method of using CFD analyses to select an acceptable set of aerodynamic design parameters (both geometric and fluid dynamic) for complex designs typical of those encountered in an aerodynamic test facility. The ultimate goal of the research is to optimize the design of a complex three-dimensional configuration such as illustrated in Figure 1.

The forebody simulator design problem possesses several interesting features in that (1) the flow-field constraints are imposed at a location away from the geometric surface that is being optimized; (2) both fluid dynamic and geometric design variables must be optimized; (3) discontinuous or localized high gradient behavior may occur within the design space (e.g., shocks or onset of separated flow); and (4) a history of prior, similar designs does not exist. These characteristics do not constitute a well-posed inverse design problem; however, the imposition of flow-field data, in the described manner, does properly define a direct optimization problem. Since flow-field data are prescribed at a known reference plane, it is possible to define an objective function that measures a norm between the reference plane flow properties associated with a particular design point (set of independent design variable values) and the desired reference plane flow properties. Since the norm is a function of the given design variables, the optimization task is to determine the particular values of these variables that produce a minimum value for the objective function.

The developed design optimization method must be extensively verified against known solutions to demonstrate the utility and applicability of the method. As a preliminary evaluation of the applied optimization algorithm, several algebraic functions are optimized and compared with previously published results. The developed design optimization technique is also evaluated by solving a series of aerodynamic test problems where the optimal solution is defined computationally, thus establishing an absolute global minimum within the allowable design space. After defining target reference plane profiles from the known optimum, the design variables are perturbed to an initial starting point and an optimization algorithm is applied to redesign the optimum configuration. The aerodynamic examples presented include a NACA0012 airfoil, convergent/divergent nozzles, and a planar supersonic forebody simulator. Although the method applied herein is applicable to either viscous or inviscid flows, only one viscous example is presented because of the increased computational expense required for a viscous CFD analysis.

This dissertation is organized such that a brief literature survey is presented in Section 2. In Section 3 the design optimization technique is developed and presented. The design technique is demonstrated by application to several aerodynamic examples in Section 4. Lastly, some conclusions relative to design optimization using the developed technique and some recommendations for future research are presented in Sections 5 and 6.

2.0 LITERATURE SURVEY

Using CFD to optimize aerodynamic designs is currently an active research topic in the applied mathematics and engineering disciplines. The motivation for developing and using these optimization methods in the design process is to reduce the overall computational effort needed to develop aerodynamic components and configurations, which will optimize a selected measure of aerodynamic performance. Several examples of aerodynamic design optimizations exist in recent literature, such as the design of airfoils, turbomachinery cascades, ducts, and nozzles. The following brief literature survey is an acknowledgment to the authors whose published work has contributed to this research. It is not intended to completely cover all of the available literature relating to optimization techniques as applied to aerodynamic design, but is intended to introduce the particular techniques that provided the background necessary to conduct this research.

The implementation of optimized aerodynamic design generally follows one of three approaches: (1) inverse design methods, (2) basis function optimization methods, and (3) direct function optimization methods. Generally, true inverse design methods are more efficient than either the basis function approach or direct optimization since the determination of the optimal design is made as an integral part of the CFD analysis. However, since many aerodynamic design problems cannot be cast in an inverse form, direct optimization methods and basis function methods are often applied.

In a typical CFD analysis problem, all geometries within the domain of interest are defined, and the spatial coordinates within the domain serve, in conjunction with time, as the independent variables. Flow properties within the domain represent the dependent variables and are determined iteratively during the solution process. An inverse design technique is one in which a flow property, typically pressure, is specified independently upon a geometric surface within the domain, and the particular geometric shape required to produce the specified property distribution is then computed as a dependent variable. Thus, the roles of dependent and independent variables are interchanged upon the surface that is to be optimally designed.

Zannetti [3] incorporated an inverse design boundary condition into a time-dependent Euler solver based upon McCormack's predictor-corrector scheme [4] to efficiently design two-dimensional airfoils, diffusers, and nozzles. Zannetti and Pandolfi [5] incorporated a similar inverse design capability into an Euler code, based upon the lambda-scheme introduced by Moretti [6], and applied their inverse method to the design of airfoil cascades. Yang and Ntone [7] were able to perform inverse design computations for subsonic nozzles and subsonic compressor cascades while solving the thin-layer Navier-Stokes equations. Each of the preceding references optimized a previously poorly defined geometry by solving a true inverse problem. During the iterative solution of the governing set of fluid dynamic conservation equations, the geometry was allowed to change at each temporal iteration until both the optimal geometry was determined and the corresponding steady-state flow-field was obtained. Using this technique to optimize an unknown geometry was very efficient since the governing set of fluid dynamic equations was necessarily being solved iteratively to obtain a steady-state flow-field analysis. One complete analysis thus yielded both the optimal geometric design and the desired steady-state CFD solution. However, in this type of formulation, the flow-field constraints, which govern the optimization problem, must be imposed on the surface that is optimized. For aerodynamic design problems in which the flow-field constraints are imposed at a location away from the optimized surface, this approach is not directly applicable.

Another aerodynamic optimization technique is the basis function approach introduced by Vanderplaats [8] and applied to airfoil optimization. Barger [9] and Barger and

Moitra [10] applied a variation of Vanderplaats' technique to develop their design-by-analysis algorithm for airfoil design. Pittman [11] also developed a similar capability as did Aidala, Davis, and Mason [12] and Davis [13,14]. Each of these references document an efficient aerodynamic design optimization for the design problems considered. However, the published applications of this method have been limited to design problems for which an extensive data base of prior designs existed to form the basis functions. Applications of this method were for examples where the optimum represented a relatively small perturbation to the predefined basis functions. Thus, an optimal combination of the basis functions produced an effective optimization technique because the allowable solution space was well defined. However, this technique is not expected to be as effective for an arbitrary aerodynamic design problem starting from arbitrary initial conditions with little prior knowledge about the optimal solution and does not appear to be a viable algorithm for the type of design optimizations considered in this research.

In direct function optimization techniques, as applied to CFD, the design problem is formulated as a general function optimization utilizing CFD to provide all necessary function evaluations that are required by the optimization algorithm. Madabhushi, Levy, and Pincus [15] developed a direct optimization design technique by formulating a general nonlinear optimization problem with application to optimal subsonic duct design. The primary application was to design curved ducts with a minimum total pressure loss between the inlet and exit planes. A quasi-Newton optimization algorithm was coupled with a spatially parabolized Navier-Stokes analysis code to minimize the objective function. The function minimized was a measure of the duct total pressure loss. A quasi-Newton optimization algorithm was selected that required an initial finite difference approximation to both the Hessian matrix (matrix of second partial derivatives) and to the Jacobian matrix (matrix of first partial derivatives). CFD analyses were used to provide the function evaluations required to form the finite difference approximations. Subsequently, the Hessian matrix was updated approximately at each new function evaluation without re-application of finite differences, but the Jacobian matrix was recomputed by finite differences at each iteration. Eliminating the need to recompute the Hessian at each iteration by finite differencing greatly reduced the total number of function evaluations necessary to converge to the optimum, as was demonstrated by comparison to other optimization algorithms.

As a general observation, both true inverse methods and the basis function methods are more efficient than an equivalent direct function optimization. However, an application such as the free-jet forebody simulator illustrated in Figure 1, is too general for either of these methods to be successfully applied. Almost any design problem can be cast as a direct function optimization if a tangible measure of the design's quality can be identified to define an objective function that is responsive to changes in the selected design parameters. Thus, the implementation of a direct aerodynamic optimization technique is investigated and reported herein as well as in References 16 and 17. It is recognized that the penalty for this generality is a potentially less efficient optimization method for some of the simpler applications that may be of interest such as airfoils and supersonic nozzles.

With current computer technology and CFD algorithms, many complex two-dimensional and some three-dimensional aerodynamic designs can be adequately analyzed, although the computational cost is quite high. Applying an optimization method that uses CFD to provide function evaluations will, by definition, be computationally expensive since multiple CFD analyses are required. Even so, for problems such as the previously described forebody simulator, some form of design optimization is required because the cost of the available alternatives (e.g., experimental "cut and try" in a wind tunnel using an inlet/forebody simulator model) may be even more prohibitive. Additionally, investigation of a more general aerodynamic design optimization technique will help prepare the way for future enhancements as computer hardware, CFD algorithms, and optimization algorithms become more efficient.

3.0 NUMERICAL TECHNIQUE

Within this research, the direct optimization problem was formulated as a nonlinear least-squares minimization utilizing existing CFD analysis codes to provide the function evaluations required by the optimization algorithm. Both Gauss-Newton and quasi-Newton optimization algorithms were applied to minimize the least-squares objective function. The optimization algorithms were coupled with the CFD analysis code as illustrated in Figure 2 to yield the desired interaction between the CFD analysis capability and the design optimization algorithm. The optimization code was kept distinct from the CFD analysis code to provide the analyst with the flexibility to select the best and most appropriate CFD analysis technique for a given design problem.

Implementation of this optimization technique involved three primary problems, (1) method of function evaluation, (2) selection and implementation of the optimization algorithm, and (3) specification of the design parameters. Each of these items is discussed in the remainder of this section.

3.1 Objective Function Evaluation

In selecting the type of CFD analysis to utilize in evaluating the objective function, the anticipated flow regime to be encountered computationally was identified [2]. A typical free-jet test envelope can range from low subsonic flow to moderately high supersonic flows, potentially with the free-jet nozzle inclined at high angles of attack relative to the test article. The appropriate aerodynamic analysis for the motivating problem requires a complex, three-dimensional, flow-field computation, necessitating the application of an Euler code or a Navier-Stokes code to produce an accurate simulation. Whether an Euler simulation is adequate, or whether a Navier-Stokes simulation is necessary is being determined in related research. However, by formulating the direct optimization problem as a nonlinear least-squares minimization, the particular flow-field analysis technique applied is irrelevant to the construction of the optimization algorithm as long as consistent and repeatable function evaluations are obtained. The flow-field simulation must be consistent and repeatable in the sense that small perturbations to design parameters are accurately reflected in the flow-field solution. This is important because the implemented optimization algorithm uses these function evaluations to compute design space gradients. If these gradients are inaccurate, then obviously the algorithm would not converge to the correct solution.

The direct optimization design method, as implemented, was developed to be independent of any particular CFD code and can be coupled as desired with any appropriate CFD technique. Although the application may require use of an elaborate Euler or Navier-Stokes solver, other less aerodynamically complex designs may be analyzed by such methods as potential flow solvers, method-of-characteristics techniques, thin-layer Navier-Stokes codes, or parabolized Navier-Stokes codes.

Within this dissertation all of the CFD analyses were performed by application of PARC, a general purpose, finite difference Euler/Navier-Stokes CFD code [18]. The version of this CFD code applicable to axisymmetric and two-dimensional configurations is referred to as PARC2D. The analogous three-dimensional CFD code is referred to as PARC3D. The PARC codes have been applied at the AEDC and elsewhere to analyze a variety of complex internal and external fluid mechanics problems [19-21]. This particular CFD code was selected because of its robustness, ease of use, and reliability. It produces consistent and repeatable flow simulations in the sense that small perturbations to design parameters are accurately reflected in the flow solution. All of the two-dimensional computational grids utilized herein were generated by the application of the INGRID code developed by Soni [22].

The purpose of this research was not to demonstrate how well a given CFD code can simulate a particular aerodynamic phenomenon or to improve CFD analysis capability per se, but to demonstrate that CFD can be coupled with efficient optimization methods to produce a potentially viable technique for optimizing aerodynamic designs that may be too complex to design by other available means. In the aerodynamic examples presented herein, no effort was made to obtain the most accurate CFD simulation for the given configuration. Whenever possible, a minimum number of grid points were applied to reduce computation time. No studies were made, for example, to assess effects of grid distribution on the CFD simulation. However, it was necessary to monitor the level of convergence, particularly at the reference plane, of each simulation used. It was necessary to reduce the temporal variation of flow variables at the reference plane, and this was accomplished by iterating on the flow field until the norm of the conservation variables at the reference plane was relatively stationary, typically to eight significant figures. To compute accurate design space gradients at the reference plane, the dominant change in the residual must be attributable to the change in the design parameters. Demonstrating that CFD can be used, as described, within an optimization algorithm for aerodynamically complex configurations will extend current capabilities in aerodynamic design optimization.

3.2 Optimization Algorithm

In the motivating design problem, the desired fluid dynamic state is completely known at the reference plane. The design requirement is to minimize the error norm between these quantities and reference plane values computed for a particular design point. The norm was selected to be an L_2 norm of the deviation between the target flow-field variables and the values computed for a given design point. The nonlinear least-squares form was selected because (1) the method is very versatile, (2) extensive literature is available on general nonlinear least-squares minimization, and (3) efficient Gauss-Newton and quasi-Newton methods are well documented for the nonlinear least-squares problem.

The nonlinear least-squares minimization was formulated as follows: Let the residuals $r_i(P_1,...,P_M)$, $i=1,2,...,N$, be functions of M design parameters, where r_i denotes the difference between the N specified reference plane quantities and the corresponding N quantities associated with the M parameters. The design parameters may be geometric, fluid dynamic, or both. To minimize r_i, in the least-squares sense, values for the parameters, P_j, are found that minimize

$$F(P_1, P_2, \ldots, P_M) = \sum_{i=1}^{N} \{r_i(P_1, P_2, \ldots, P_M)\}^2 \tag{3.2.1}$$

This sum can be written in vector form as $\underline{R}(\underline{P})^T \underline{R}(\underline{P})$ where $\underline{R}(\underline{P})$ denotes a vector with components r_i, which are functions of the parameters $\underline{P}$.

Three sets of fluid dynamic variables were considered to specify the reference plane state including, (1) the Navier-Stokes dependent variables in conservation form, (2) the Navier-Stokes dependent variables in nonconservation form, and (3) RP total conditions and directional Mach number. Preliminary studies conducted in this research using a simple airfoil optimization problem detected no significant difference in results caused by the choice of dependent variables.

Except when otherwise noted, the set of variables used herein to define the reference plane fluid state are (1) RP total pressure, $p_{T_{rp}}$, (2) RP total temperature, $T_{T_{rp}}$, and (3) RP directional Mach number, $M_{x_{rp}}$, $M_{y_{rp}}$, and $M_{z_{rp}}$. In two dimensions, one less Mach number component is required.

Variable constraints, when applied, are imposed by adding a barrier function, such as the inverse function [23], to the objective function. Thus, the expression $\underline{R}^T\underline{R}$ becomes

$$\underline{R}^T\underline{R} = \sum_{i=1}^{N_r}\{\left(P_{T_{rp}}-P_T\right)_i^2+\left(T_{T_{rp}}-T_T\right)_i^2+\left(M_{x_{rp}}-M_x\right)_i^2 + \left(M_{y_{rp}}-M_y\right)_i^2+\left(M_{z_{rp}}-M_z\right)_i^2\} + \sum_{j=1}^{N_c}\phi_j^2 \tag{3.2.2}$$

where N_r is the number of reference plane points, ϕ, represents the imposed constraint functions, and N_C is the number of imposed constraints. Since each term in Eq. (3.2.2) contains five residual fluid dynamic components, in order to put this in the form of Eq. (3.2.1), $N=5N_r+N_C$ must hold. In Eq. (3.2.2) the subscript rp denotes the specified reference plane values while unsubscripted values denote reference plane values computed for a particular trial design (set of design parameters). Quantities in Eq. (3.2.2) are normalized by appropriate reference quantities to produce target reference plane values of order one.

A popular and efficient algorithm for minimizing the nonlinear least-squares form, Eq. (3.2.1), is the Gauss-Newton method [23] or one of its variants such as Hartley's modified Gauss-Newton method [24]. An advantage of these small residual algorithms as applied to the least-squares form is the elimination of the need for the

Hessian matrix in the algorithm formulation. Formation of the Hessian matrix requires specification and evaluation of N*M*(M+1)/2 second derivative terms. For the motivating application, computation of the Hessian matrix is prohibitively expensive because these derivatives must be approximated by finite differences. Derivation of the Gauss-Newton method, applied to the least-squares problem, is available from several sources [23,24] but is repeated in Appendix B.

Applying the Gauss-Newton method to minimize Eq. (3.2.1) yields an optimization algorithm of the form

$$J^T J \Delta \underline{P} = -J^T \underline{R} \tag{3.2.3}$$

where J denotes the Jacobian of $\underline{R}$ with respect to $\underline{P}$ defined by

$$J = \begin{pmatrix} \dfrac{\partial r_1}{\partial P_1} & \cdots & \dfrac{\partial r_1}{\partial P_M} \\ \cdot & & \cdot \\ \cdot & & \cdot \\ \cdot & & \cdot \\ \dfrac{\partial r_N}{\partial P_1} & \cdots & \dfrac{\partial r_N}{\partial P_M} \end{pmatrix} \tag{3.2.4}$$

Equation (3.2.3) defines an M-by-M system of equations that was used to compute the change, $\Delta\underline{P}$, in the design parameter solution vector, $\underline{P}$. To apply this algorithm, J was evaluated by finite difference approximation to obtain the partial derivative of each residual component with respect to each design parameter. This requires M+1 function evaluations to compute the M partials for each residual. Since a CFD solution was used to obtain each function evaluation, approximation of this Jacobian was by far the most expensive part of the algorithm.

An extension of this algorithm is Broyden's quasi-Newton method [23,25]. Broyden's extension modifies the standard Gauss-Newton method by approximating the Jacobian, J, at the k+1 iteration strictly from the Jacobian and other data available at iteration k rather than recomputing J directly. Since, in quasi-Newton algorithms, a finite difference approximation to J is made only for the initial iteration, the accuracy of this approximation is even more important than for the Gauss-Newton technique. If the quasi-Newton algorithm is to converge to the optimal solution, an accurate initial approximation to J must be made. Applying Broyden's quasi-Newton method yields an optimization algorithm identical in form with the Gauss-Newton method, Eq. (3.2.3), and is given by

$$B^T B \Delta \underline{P} = -B^T \underline{R} \qquad (3.2.5)$$

where the Jacobian approximation, B_k at iteration k, is updated for iteration k+1 according to

$$B_{k+1} = B_k + \frac{(\Delta \underline{R}_k - B_k \Delta \underline{P}_k)\Delta \underline{P}_k^T}{(\Delta \underline{P}_k^T \Delta \underline{P}_k)} \tag{3.2.6}$$

where B_0 is obtained by a finite difference approximation to the Jacobian. This modification to the Gauss-Newton algorithm is based upon the Jacobian approximation developed by Broyden [25], the derivation of which is repeated in Appendix C. One of the key assumptions used to derive Eq. (3.2.6) is that the residual change in directions orthogonal to the direction $\Delta \underline{P}_k$ predicted by B_{k+1} is identical to that predicted by B_k. The imposition of the quasi-Newton condition, which constrains B_{k+1} to hold exact derivative information in the direction of $\Delta \underline{P}_k$ for linear $\underline{R}$, provides the other conditions necessary to uniquely determine B_{k+1}. Application of the Gauss-Newton algorithm requires M+1 function evaluations for each iteration since the Jacobian is approximated by finite differences, whereas Broyden's extension requires M+1 function evaluations for the first iteration but only one evaluation for subsequent iterations. Thus, if the quasi-Newton method can be applied, after the first iteration M function evaluations are eliminated at each iteration. For typical aerodynamic optimization problems, the function evaluation is the dominant part of the cost and a significant savings is realized whenever the quasi-Newton algorithm can be applied.

It is well known that the Gauss-Newton method, using analytical derivatives, determines a search direction that guarantees a reduction in the objective function for some step-size in that search direction [24]. Thus, a linear search technique is often employed once the search direction is determined by either the Gauss-Newton or quasi-Newton algorithm. The greatest benefit is derived from the linear search whenever the full correction computed by the optimization algorithm fails to produce a reduction in the objective function value. Because of the expense of function evaluations, a comparatively simple method, following Hartley [24], was applied herein. When applying Hartley's technique, one function evaluation, in addition to the evaluation at the predicted optimum, was made in the determined search direction. The base design point and the two new design points along the search direction were then used to define a quadratic interpolation function which was analytically solved to yield the optimal design parameters within the search interval.

The linear search adds at least one additional function evaluation per iteration in anticipation that the overall number of iterations will be reduced. Because of the expense of function evaluations, the linear search was employed only when a full optimization step failed to produce a reduction in the objective function. The linear search strategy is described more fully in Appendix D.

3.3 Design Parameters

For the problem of interest, pertinent design variables are the free-jet fluid dynamic parameters and the variable forebody simulator geometry. The free-jet parameters, considered herein, are jet total pressure, jet total temperature, and jet Mach number. To produce an efficient optimization method, the forebody simulator geometry was described parametrically to reduce the total number of design variables. For two-dimensional applications, a parametric polynomial representation of two dimensional curves as given by the Bernstein-Bezier polynomial [26] was applied as follows:

$$\underline{x}(u) = \sum_{i=0}^{n} \frac{n!}{(n-i)!\,i!} u^{i}(1-u)^{(n-i)} \underline{x}_{i}; \quad 0 \le u \le 1 \tag{3.3.1}$$

where $\underline{x}_0$, $\underline{x}_1$, $\underline{x}_2$, ... , $\underline{x}_n$ denote the position vectors of the n+1 geometric control points. In this form the defined curve passes identically through the control points defined by vectors $\underline{x}_0$ and $\underline{x}_n$ but not through the remaining control points. This allows a high degree of variability for a given number of design parameters relative to other parametric representations with the penalty of making the influence of each parameter upon the total curve somewhat obscure. Application of the Bezier polynomials prevents the large oscillations encountered when using interpolating polynomials because of the "convex hull" property of Bezier polynomials. This property ensures that the Bezier polynomial lies within the polygon formed by connecting the vertices of each of the Bezier control vectors.

For three-dimensional applications, an extension of Eq. (3.3.1) defining Bezier surfaces [26] was applied. The Bezier surfaces and interior were defined as follows:

$$\underline{x}(u,v,w) = \sum_{i=0}^{p} \sum_{j=0}^{q} \sum_{k=0}^{r} g_i^p(u) g_j^q(v) g_k^r(w) \underline{x}_{ijk} \tag{3.3.2}$$

Here $\underline{x}_{ijk}$ denotes the position vectors of the control points, $g_i^p(u)$, $g_j^q(v)$, and $g_k^r(w)$ are Bernstein basis functions of degree p,q, and r, respectively, whereas u,v, and w are parameters which range from 0 to 1. The Bernstein basis functions, $g_i^p(u)$, are defined by

$$g_i^p(u) = \frac{p!}{(p-i)!\,i!} u^i (1-u)^{(p-i)} \quad ; i = 0,1,2,\ldots p \tag{3.3.3}$$

with the other basis functions analogously defined.

The set of design variables are of diverse type, including both geometric parameters and fluid dynamic parameters. Thus, each variable was nondimensionalized by an appropriate reference quantity. The nondimensionalization was chosen to make each design variable nominally of order one.

4.0 NUMERICAL EXAMPLES

The aerodynamic design optimization technique was evaluated by optimizing a series of numerical examples including, (1) algebraic test functions, (2) a NACA0012 airfoil in inviscid flow, (3) a NACA0012 airfoil in viscous flow, (4) a planar inviscid flow in a convergent/divergent nozzle, (5) a three-dimensional inviscid flow in a nozzle, and (6) an inviscid supersonic flow past a planar, forebody simulator. In each of these examples, the optimization problem was formulated such that a global minimum exists within the solution space. The evaluation criterion was to quantify the number of function evaluations required to determine the optimum.

The primary goal of this research was to demonstrate the feasibility of coupling CFD analyses capability with nonlinear optimization methods to produce an aerodynamic design technique. However, if the developed design method is to be successfully applied, it must also be efficient. For the subject application, efficiency can be equated with minimizing the total number of function evaluations required to isolate the optimum since this is where the preponderance of the computational cost is incurred. In fact, typical computer times required to evaluate the objective function, using an Euler or Navier-Stokes solver on a supercomputer, may range from several computer minutes for a simple two-dimensional design to computer hours for a complex three-dimensional design with large amounts of computer memory required. The optimization algorithm applied, which utilized the function evaluations, typically executed in five to ten seconds on a CRAY XMP supercomputer. The number of function evaluations was minimized herein by selecting an efficient optimization algorithm and applying an effective geometric parameterization to reduce the number of design variables.

4.1 Algebraic Test Functions

Madabhushi, Levy, and Pincus [15] developed a coupled direct optimization/CFD design method in which an objective function, defined as the average duct total pressure loss, was minimized as a general nonlinear function. The function minimizations were made by applying the Broyden, Fletcher, Goldfarb and Shanno (BFGS) quasi-Newton algorithm. The selection of this quasi-Newton algorithm was based, in part, upon a comparison of the relative performance of the BFGS algorithm, a conjugate gradient algorithm, and a gradient algorithm as applied to the minimization of ten algebraic test functions. The relative performance of the algorithms was measured by comparing the total number of function evaluations required for each method to converge to the global minimum.

These test functions were also used herein to compare the relative efficiency of the Gauss-Newton algorithm and a mixed Broyden/Gauss-Newton algorithm with the results of Madabhushi et al. The mixed Broyden/Gauss-Newton method refers to a modified version of the standard Broyden algorithm, which switched to a standard Gauss-Newton step every ten iterations. In practice this tends to minimize the potentially adverse effects that poor initial approximations of the Jacobian may have upon the quasi-Newton algorithm's solution characteristics, at the expense of periodically recomputing the Jacobian matrix.

The goal of this comparison was to demonstrate that the optimization technique applied herein is reasonably efficient relative to other available optimization algorithms. If the comparisons are favorable, then the ease of application and versatility afforded by the nonlinear least-squares formulation makes this an attractive technique for application to aerodynamic design optimization. Reiterating a further advantage of the least-squares form applied herein, the need for computation of the matrix of second partial derivatives (Hessian matrix) with respect to each design variable is eliminated. Since these derivatives are not available analytically, computation of the Hessian represents both an expensive computation and a potentially unreliable computation because of potential inaccuracy in the objective function evaluation.

The test functions selected by Madabhushi et al., exhibit a broad range of functional behavior so that an algorithm that satisfactorily optimizes these functions can be expected to be a reliable general purpose algorithm. Since the functional behavior of the subject objective function is not known a priori, it is important to apply a versatile optimization algorithm. The first five of the test functions represent classic examples, which are devised to pose particular difficulties for optimization methods and are documented in several sources [i.e. 23,27]. Typical characteristics are a steep valley, a near stationary point within the solution space, or singularities within the Hessian matrix. These functional characteristics typically can cause an optimization algorithm to converge slowly or in some cases converge to a local optimum rather than the desired global optimum. The other five test functions were selected to include a more typical range of multivariate polynomials to evaluate an algorithm's performance for more commonly encountered functional forms [15]. A brief description of each of the ten functions, the optimization starting point, and the location and value of the minimum is presented in Reference 15, and is repeated in Appendix E for the reader's convenience. Also included in Appendix E is the equivalent least-squares form for each function. This is the same form to be optimized in subsequent aerodynamic examples.

Table 1 presents the number of function evaluations needed to locate the minimum of the test functions for both the Gauss-Newton algorithm and the mixed Broyden/Gauss-Newton algorithm compared to the best results for the BFGS algorithm reported in Reference 15. Results are presented for two different convergence criteria. The first criterion (C1) requires (1) functional value change of less than 10^{-12}, (2) solution vector change of less than 10^{-6}, and (3) solution gradient change of less than 10^{-4} for a given iteration. The second criterion (C2) requires only that the function minimum be located within 10^{-4}. Both criteria are used because of an ambiguity in Reference 15. The cited reference indicates that criterion C2 was used within the research, although private correspondence with one of the authors indicated that criterion C1 was used to determine convergence.

For eight of the ten test functions, the nonlinear least-squares minimization was successful. In fact, the results were generally better than those obtained by the

Table 1

ALGORITHM COMPARISON: NUMBER OF FUNCTION EVALUATIONS

	GAUSS-NEWTON		BROYDEN/ GAUSS-NEWTON		BFGS
FUNCTION	C1	C2	C1	C2	
ROSENBROCK	95	92	79	78	85
HELIX	45	37	41	38	105
WOODS	L.M.	L.M.	L.M.	L.M.	110
SINGULAR	111	81	42	35	121
BIGGS	Failed	Failed	Failed	Failed	86
POLYNOMIAL #1	85	61	37	30	22
POLYNOMIAL #2	73	49	137	131	71
POLYNOMIAL #3	89	61	39	31	41
POLYNOMIAL #4	116	86	48	36	198
POLYNOMIAL #5	116	86	48	36	175

L.M. => Converged to a local minimum

BFGS algorithm. However, for the Woods function, both of the least-squares algorithms applied herein located the strong local minimum noted in Appendix E. When the initial guess was changed to almost any other value, then the global minimum was isolated in a number of function evaluations comparable to Reference 15. For the Biggs function neither the Gauss-Newton nor quasi-Newton algorithm was able to converge to the correct solution starting at the published initial guess. Again, when some other initial guess was chosen, one of the two global minima was isolated.

None of the three methods compared was clearly superior. The nonlinear least-squares algorithms were generally more efficient than the BFGS method for the problems in which they worked, where efficiency was measured by the total number of function evaluations required to reach the optimum. The BFGS algorithm was able to successfully solve two problems for which the least-squares algorithms failed. However, it should be emphasized that both of these examples present extremely adverse functional behavior to any optimization algorithm. Because of the previously stated advantages of the least-squares form and the reasonable performance upon the algebraic test functions, it was concluded that further evaluation of the nonlinear least-squares approach by application to aerodynamic optimization test problems was warranted.

The comparisons made in Table 1 were of a general nature and were used to provide a crude indication of how well the Gauss-Newton and quasi-Newton algorithms perform relative to more recently developed optimization algorithms, such as the BFGS. No attempt was made to "tune" the least-squares algorithms to enhance their relative performance. All derivatives were evaluated by forward differences with some minor variation in algorithm performance as a function of derivative accuracy attributable to variation in parameter step size detected. Additional variation was detected in the mixed algorithm as a function of the frequency with which a full Gauss-Newton step is taken. These observations were not investigated further because the purpose of the algebraic test problems was only to provide a general assessment of the selected nonlinear least-squares algorithms, not to identify the best algorithm for minimizing algebraic functions of a particular type.

Since the motivating design problem may require ten or more design variables, linear combinations of the previously described algebraic test functions were optimized to determine whether the algorithm performance degraded for larger numbers of independent variables. No fundamental difference in performance was noted for optimization problems with up to fifteen independent variables.

4.2 Inviscid Flow About a Planar Airfoil

Optimization of a planar airfoil in inviscid flow by specifying "reference plane" (RP) values at a station downstream of a NACA0012 airfoil (Fig. 3) provides an illustration of the design optimization technique. The RP was located at a vertical plane beginning at the airfoil trailing edge and extending five chord lengths into the computational domain. The NACA0012 airfoil is a well-known airfoil contour that has been extensively analyzed and is defined by

$$y(x)=5t(0.2969x^{1/2}-0.126x-0.3516x^2 +0.2843x^3-0.1015x^4) \tag{4.2.1}$$

where the parameter, t, specifies the airfoil thickness. For the NACA0012 airfoil the thickness parameter is specified as 0.12 for a chord length of 1.0089. This airfoil contour provided a convenient definition of a one parameter design optimization problem for which the CFD analysis was quite simple. The purpose of this example was to provide an aerodynamically simple design problem to demonstrate that it is possible to optimize an aerodynamic surface by specifying the fluid dynamic state at a RP remote to that surface.

The PARC2D CFD code was used to define the target RP properties by computing the inviscid flow field about this airfoil, subject to the boundary conditions indicated in Figure 3 using 9,000 grid points to resolve the domain. Free-stream properties were held constant at a Mach number of 0.8 a distance of five to ten chord lengths away from the airfoil surface. Static pressure corresponding to the specified free-stream Mach number was specified at the indicated computational exit plane. The RP was located at the airfoil trailing edge and extends to the boundary of the computational domain, even though the influence of the body was minimal at approximately two chord lengths into the domain. The RP properties used to form the nonlinear least-squares objective function, as defined by Eq. (3.2.2), were minimized by application of Broyden's algorithm.

No effort was made to obtain a highly accurate CFD simulation. However, each simulation was scrutinized to assure that the solution, particularly at the RP, was strongly converged. In this example, each PARC2D solution was converged until the norm of the RP conservation variables was constant to eight significant figures. For this simple problem the CFD results were consistent with those obtained by Jameson and Mavriplis [28], among others, as evidenced by the pressure coefficient distribution along the airfoil surface (Fig. 4).

To initialize the optimization, the airfoil thickness was arbitrarily perturbed to 1/12 of its original value as an initial guess. This produced a very flat airfoil, which was obviously distinct from the target profile and thus produced a significant perturbation at the RP. In fact, as seen from the surface pressure profile (Fig. 4), the target airfoil is mildly transonic with the anticipated shock at the airfoil surface. Conversely, the almost flat profile used for an initial guess produced very little distortion of the free-stream with the flow field remaining subsonic throughout the domain.

The optimal design parameter was derived by applying Broyden's quasi-Newton algorithm. For the first iteration, the Jacobian, J, was approximated by a one-sided finite difference of each of the N residuals as in the following example for the partial derivative of the i^{th} residual with respect to the design parameter, t,

$$\frac{\partial r_i}{\partial t} = \frac{r_i(t+\Delta t) - r_i(t)}{\Delta t} \qquad (4.2.2)$$

Since a quasi-Newton algorithm was applied, a good approximation to the design space Jacobian was required at the first iteration. This Jacobian was not recomputed at subsequent iterations but was updated approximately according to Eq. (3.2.6).

To give an indication of the accuracy of this Jacobian, and to illustrate that stable computation of derivatives was possible for this problem, an investigation of derivative accuracy versus the size of Δt used in Eq. (4.2.2) was performed. Figure 5 shows the variation of the normalized objective function derivative with respect to the design parameter versus the log of the parameter step size for first-order forward differences as given by Eq. (4.2.2). This gradient of the objective function was used to provide a crude assessment of the partial derivatives of the residual components that were used in the optimization algorithm. Although this does not provide detailed information about variation of individual residual derivatives, it does provide a means of measuring global variation at the RP. As can be seen, this derivative was sensitive to step size, but approached a constant value for step sizes less than 0.001. In fact, the actual data indicated that the derivative was constant within 0.5 of 1 percent for step sizes less than 0.001. Based upon this analysis, a step size of 0.001 was selected for the design parameter.

Figure 6 compares the target geometric profile with the initial guess profile, the first iteration profile, and the optimal profile as determined by Broyden's algorithm. The correct geometry was obtained in four iterations, which required five function evaluations (CFD solutions). Figure 7 shows typical variation of flow variables at the RP as evidenced by Mach number profiles. Figures 8 and 9 show the reduction of the objective function and the convergence history of the design parameter, t, versus iteration number, respectively. As evidenced by these figures, the Broyden's algorithm isolated the global minimum quite efficiently. The data from which Figure 9 was produced indicates that the optimum was located within 1 percent in 2 iterations and was isolated within 0.1 of 1 percent in 4 iterations.

Airfoil optimization has been performed by several other researchers by prescribing a pressure distribution along the airfoil surface and solving a true inverse problem. As an interesting example of the versatility of the nonlinear least-squares approach, the previously described design problem was also solved by forming the least-squares objective function from the difference between the airfoil surface pressures for a given design point and a specified pressure distribution. The target pressure distribution was obtained as before by applying PARC2D to compute the inviscid flow field about this airfoil, subject to the previously described boundary conditions (Fig. 3). The airfoil surface pressure distribution was then used to form a nonlinear least-squares objective function, defined by

$$\underline{R}^T \underline{R} = \sum_{i=1}^{N} \left(P_{rp} - P \right)_i^2 \tag{4.2.3}$$

where P_{rp} denotes the desired airfoil surface pressure at one of the N RP locations and P denotes the airfoil surface pressure for a given design point. Optimization of the airfoil in this manner produced results very similar to those obtained by defining a trailing edge reference plane. This is illustrated in Figure 10 by the reduction in the objective function and in Figure 11 by the convergence of the design parameter, t. For this formulation the optimum was located within 2 percent in 4 iterations and was isolated within 0.3 of 1 percent in 6 iterations.

4.3 Viscous Flow About a Planar Airfoil

Formulating the aerodynamic design problem as a nonlinear least-squares minimization allows flexibility in selecting the type of CFD simulation as well as allowing application to complex designs. For example, inclusion of viscous effects does not necessitate any changes to the applied optimization algorithm. The difference in the overall optimization process occurs only in the CFD analysis step. In other words, a more elaborate CFD simulation provides the various function evaluations, but the optimization algorithm does not recognize that the origin of the function evaluation assumed a more complex physics model.

As a simple demonstration of a design problem in which viscous effects were included, the previously described NACA0012 airfoil was analyzed with function evaluations supplied by viscous, Navier-Stokes simulations. Analogous to the inviscid flow over the airfoil, PARC2D was used to define the target RP properties by computing viscous flow about a NACA0012 airfoil, subject to the indicated boundary conditions (Fig. 12). The imposed boundary conditions were identical to those used for the inviscid airfoil example, except the airfoil surface was modeled as a no-slip, adiabatic wall rather than an inviscid, slip-wall boundary. A free-stream Reynolds number of 10^6, based upon chord length, was specified, which produced an attached laminar boundary layer (Fig. 13) when analyzed with PARC2D. In this example the RP was extended three chord lengths into the domain from the airfoil trailing edge. The design parameter (airfoil thickness) was perturbed to 1/12 its original value as an initial guess to begin the optimization. Broyden's quasi-Newton algorithm was then applied to derive the optimal value of the parameter. Because of the similarity to the inviscid problem, no sensitivity study of the design variable was performed.

Figure 14 compares the target geometric profile with the initial guess profile, the first iteration profile, and the optimal profile as determined by Broyden's algorithm. The correct geometry was obtained in three iterations, which required five function evaluations (CFD solutions). Figures 15 and 16 show the reduction of the objective function and the convergence history of the design parameter, t, to the known optimum. Again, Broyden's algorithm isolated the global minimum very efficiently. The data from which Figure 16 was produced indicates that the optimum was located within 1 percent in 2 iterations and was isolated within 0.1 of 1 percent in 3 iterations.

This viscous example was modified by choosing an initial guess for the design parameter that was double the correct value, producing a much thicker initial airfoil contour. This posed a more difficult optimization problem because the computed flow field about the initial guess airfoil was separated (Fig. 17), whereas the computed flow field about the target airfoil was attached for the prescribed boundary conditions (Fig. 13). The absence or presence of separated flow within the design space provided an abrupt change in the flow field for candidate designs in very nearly a discontinuous fashion. To assess whether the optimization technique is robust enough to optimize designs for which flow separation may occur, this airfoil was analyzed with the RP deliberately placed within the region of separated flow. The RP was located at the trailing edge and extended from the airfoil surface to the edge of the computational domain. As with prior examples, PARC2D was used to provide function evaluations at the RP.

Convergence for this example was similar to earlier results, although somewhat slower, with the optimum design variable located within 1 percent in 5 iterations and to within 0.1 of 1 percent in 6 iterations requiring 7 function evaluations. Figure 18 illustrates the convergence to the target geometry by comparing the target geometric profile with the initial guess profile, the first iteration profile, and the optimal profile as determined by Broyden's algorithm. Figures 19 and 20 illustrate the reduction of the objective function and the convergence of the design parameter, t, to the known optimum, respectively. The prominent slope change in Figure 19 coincides with the first candidate design for which minimal separated flow was present.

4.4 Inviscid Planar Convergent/Divergent Nozzle Flow

Optimization of multiple aerodynamic design parameters was illustrated by analyzing inviscid, planar, supersonic flow in a nozzle (Fig. 21). The design variables for this problem were inflow total pressure, inflow total temperature, and the nozzle wall contour defined as a three parameter Bezier curve. The vectors used to define the Bezier curve were located axially at the inlet plane, the midpoint, and the exit plane as indicated in Figure 21. The exit plane control vector was held constant during the optimization. The 'y' coordinate of the other two vectors were allowed to vary as design parameters during the optimization (Fig. 21). In addition to these two geometric parameters, the nozzle inlet total temperature and the nozzle inlet total pressure were allowed to vary, yielding a total of four design parameters. Each parameter was nondimensionalized by an appropriate reference quantity. The Bezier parameters were normalized by the target nozzle inlet height, total pressure by the target total pressure, and total temperature by the target total temperature.

The simultaneous variation of inlet total conditions and nozzle wall contour is not necessarily representative of a typical nozzle design problem, but this example was constructed because simultaneous variation of free-jet total conditions and a variable geometry occurs with the supersonic forebody simulator design problem that motivated the present research. The target solution was defined by selecting the Bezier parameters to produce a nominal 2:1 area ratio nozzle and applying PARC2D to solve the Euler equations within the domain using 1,600 grid points to resolve the domain. To form an initial guess, the inflow height and the nozzle throat height were reduced such that the initial nozzle area ratio was approximately doubled and the nozzle throat was shifted forward. The initial guess inflow total temperature and total pressure values were doubled. The disparity between the target design and the initial guess is illustrated by comparing the centerline Mach number profiles for the target design and for the initial guess (Fig. 22). As can be seen, the exit target Mach number was nominally 50 percent below the initial guess with a corresponding variation within the rest of the nozzle. Again, no special effort was made to produce a highly accurate simulation, although results agree well with one-dimensional theory (Fig. 23).

Broyden's quasi-Newton algorithm was again applied in this example. For the first iteration, the Jacobian was approximated by a one-sided finite difference of each of the N residuals as in the following example for the partial derivative of the i^{th} residual with respect to the j^{th} parameter

$$\frac{\partial r_i}{\partial P_j} = \frac{r_i(P_1,\ldots,P_j+\Delta P_j,\ldots,P_M) - r_i(P_1,\ldots,P_j,\ldots,P_M)}{\Delta P_j} \tag{4.4.1}$$

As with the airfoil example, the partial derivative of the objective function with respect to one of the geometric design parameters was investigated by performing a sensitivity analysis based on comparing derivative accuracy versus the size of ΔP_j used in Eq. (4.4.1). Figure 24 depicts the variation of the normalized objective function differences, as given by Eq. (4.4.1), with respect to one of the Bezier design parameters, P_1, versus the log of the parameter step size. As can be seen, this derivative is sensitive to step size, but attains a constant value for step sizes between 0.0001 and 0.002. Between these limits the partial derivative is constant within 0.5 percent. The inaccuracy observed for large step sizes reflects the nonlinearity of the problem and the inaccuracy introduced by neglecting higher order terms in the difference approximation. The inaccuracy for very small step sizes results from numerical errors in the function evaluations becoming of the same order as the true difference in functional value. From this data a step size of 0.001 was selected for the Bezier parameters. For an Euler simulation, the residuals vary linearly with total temperature and total pressure; thus, these parameter step sizes are not as critical in this example. A nondimensional step size of 0.001 was selected for the fluid dynamic parameters to be consistent with the geometric parameters.

The optimization algorithm converged to the global minimum in four iterations which required nine function evaluations. Typical convergence of the reference plane properties is illustrated in Figure 25, which shows reference plane Mach number profiles for the target solution, the initial guess, the first iteration, and the optimum. The reduction in the objective function is illustrated in Figure 26. During the optimization, inflow total conditions converged to within 1 percent of the correct value in 1 iteration. This is because, for this example, RP pressures and temperatures scale linearly with the specified total conditions. Thus, the residuals vary linearly with these parameters, and rapid convergence was expected since a Gauss-Newton type algorithm was applied. In fact, for an optimization problem in which the residuals are linear in all of the parameters, it is well known that a Gauss-Newton algorithm converges to the exact solution in one iteration. The geometric parameters converged more slowly but still at an acceptable rate. The convergence of the full geometry defined by the individual parameters is illustrated in Figure 27, which shows the iterative variation of the nozzle wall contour. The convergence of the individual design parameters to the correct solution is illustrated by Figures 28 through 31.

4.5 Inviscid Three-Dimensional Nozzle Flow

A three-dimensional rectangular nozzle (Fig. 32) was used to demonstrate that the nonlinear least-squares optimization method is applicable in three dimensions. The nozzle geometry and interior grid were defined by three-dimensional Bezier polynomials, Eq. (3.3.2). Four control points were specified at each of five axial planes such that each axial cross section was rectangular. The entire volume was then defined using the coordinate vectors of these 20 control points to define the Bezier polynomials. Two design parameters were defined as coefficients, P_1 and P_2, that controlled the length and width of the rectangular cross section at the midplane (Fig. 32). The target geometry corresponded to values of unity for each parameter, which produced a nozzle with a nominal exit-to-throat area ratio of 2.5. Total conditions were specified at the nozzle inlet, and a static pressure below second critical was selected at the nozzle exit, which allowed fully supersonic flow to develop in the divergent portion of the nozzle. This geometry and boundary conditions produced a flow field with a nominal exit Mach number of 2.5 when analyzed by the application of the Euler version of the PARC3D code.

For an initial guess, the design parameters P_1 and P_2 were set equal to 2.0 and 2.5, respectively. This produced a nozzle with a nominal exit-to-throat area ratio of 64. A PARC3D analysis of this geometry subject to the described boundary conditions produced a flow field with a nominal exit Mach number of 5.8 using 23,000 grid points in the simulation. Unlike the target nozzle, which was square at each axial cross section, the initial guess nozzle had a square cross section at the inflow plane, which transitioned to a rectangular cross section at the midplane, and then transitioned again to a square at the exit plane. The large differences in exit flow conditions for the initial guess nozzle compared to the target nozzle were selected to illustrate that the initial guess flow field does not necessarily need to closely resemble the desired optimum to obtain acceptable results. The differences in the flow fields for the target nozzle and the initial guess nozzle geometries are illustrated by comparing the centerline Mach number profiles for the two designs (Fig. 33). Also presented are the distributions for the first iteration and for the computed optimum.

A sensitivity analysis was performed on design parameter P_1 which indicated that parameter step sizes ranging from 0.0001 to 0.01 produce nearly the same objective function derivative (Fig. 34). The variation in Figure 34 reflects the sensitivity to parameter step size attributable to nonlinear effects and numerical error inherent in the objective function evaluations. A value of 0.001 was selected for the design variable step size in this example. The resulting Jacobian was not accurate enough for successful application of Broyden's algorithm, but when the Gauss-Newton algorithm was applied, the RP properties converged in 6 iterations requiring 18 function evaluations. Figures 35 and 36 provide an example of the RP convergence by comparing 'y' and 'z' centerline Mach number profiles at the RP for the target solution, the initial guess, the first iteration, and the computed optimum. The achieved reduction in objective function and the design parameter convergence is depicted in Figures 37 and 38, respectively, which illustrate that the global minimum was isolated. Convergence is further demonstrated by comparing the wall contours for constant 'y' planes (Fig. 39) and constant 'z' planes (Fig. 40).

4.6 Inviscid Supersonic Flow About a Planar Forebody Simulator

A two-dimensional analog to the motivating design problem was constructed and is shown in Figure 41. The configuration shown was used to define the target flow variables at the indicated reference plane. Thirteen thousand grid points were used to resolve the domain, which was analyzed inviscidly by the application of PARC2D in the Euler mode. In this example the Mach number at the inflow plane was treated as a design variable to represent the variable free-jet Mach number, which would be encountered in the motivating design problem. The forebody simulator geometry was defined as a Bezier curve with four variable parameters. The geometric design variables were normalized by the forebody simulator height, and the Mach number design variable was normalized by the target Mach number to make each design variable of the same order. The RP was located one inlet height in front of the inlet entrance.

The target design was a relatively blunt forebody with an incoming Mach number of 3.0 (Fig. 41). The reference plane was located downstream of the detached shock emanating from the leading edge of the forebody. Also within the flow field, weak shocks reflect from the cell wall boundary and from the nozzle walls. The simulation was run with an exit pressure low enough to maintain fully supersonic flow across the computational exit plane. The five design parameters shown in Figure 41 were then perturbed to initialize the optimization. For the initial guesses, the Mach number was increased by 50 percent, and the geometric parameters were reduced by 10 to 70 percent to intentionally provide a poor initial guess. The disparity between the target design and the initial guess configuration is illustrated by comparison of the respective Mach number contours (Figures 42 and 43). As can be seen, the shock structures in front of the reference plane are quite different, leading to large discrepancies in RP flow variables. The forebody shock passes very close to the RP in the initial guess configuration, which further complicates the optimization task.

The RP objective function was minimized by the application of the Gauss-Newton algorithm. Analysis of the objective function gradients indicated that the minimum derivative variation was about 2 percent (Fig. 44) for nondimensional, geometric variable step sizes between 0.02 and 0.05. These derivatives were not accurate enough for successful application of the quasi-Newton alogorithm. However, when the Gauss-Newton algorithm was applied, convergence was obtained in 5 iterations requiring 31 function evaluations. The maximum Mach number deviation, at the RP, was less than 1 percent after only 2 optimization steps requiring 13 function evaluations, which for many applications, may be adequate. A comparison of the reference plane Mach number profiles for the initial guess, the target solution, and the final converged solution is made in Figure 45, which shows excellent agreement between the target and final solutions. Figure 46 plots the objective function versus design iteration number illustrating that the global minimum was isolated. The convergence history for each of the five design parameters is illustrated in Figure 47.

The motivating design problem requires that RP properties be matched within design tolerance while significantly shortening the actual aircraft forebody.

An example emulating this type of optimization problem was constructed by seeking a forebody half the length of the described target forebody as depicted in Figure 41. This length restriction excluded an exact match of RP variables from the optimization design space. Each candidate design was analyzed as a full test cell configuration without utilizing a plane of symmetry as with the target configuration. Each design was analyzed inviscidly by the application of the blocked version of PARC2D in the Euler mode using 26,000 grid points to resolve the domain in each CFD simulation.

The optimization problem was constructed using four design variables. The inflow plane Mach number (normalized by M=3.0 as a reference Mach number) was used as a fluid dynamic design variable. The forebody simulator geometry was again defined as a Bezier curve with the vertical component of three of the Bezier control vectors used as design variables. These geometric design variables were normalized by a reference length equal to the height of the target forebody. As with the full-length forebody design, the Gauss-Newton algorithm was applied. In 4 iterations, requiring 17 function evaluations, the deviation from normalized RP objective function components of total pressure and axial Mach number was as indicated in Figures 48 and 49 for various optimization iterations. In these figures, each RP component was normalized by the corresponding target value to facilitate comparison of the various design iterations. The target values for the vertical Mach number component were very near zero; thus, comparison of the actual residual components is most meaningful and is presented in Figure 50. The total temperature component of the objective function is not presented since total temperature remains constant, within numerical accuracy, for this inviscid computation.

As seen from Figures 48 through 50, each component of the objective function was reduced from its initial value. The convergence and rate of reduction of the total objective function is further illustrated in Figure 51. Further iterations failed to yield any appreciable reduction in the objective function. Additionally, the contribution from the total temperature components to the objective function sum became of the same order as the total pressure and Mach number components. This indicated that further reduction in the objective function was unlikely, since for the Euler simulations, any mismatch in total temperature could be attributed to numerical error. The comparison of the RP Mach number for various iterations, as shown in prior examples, is presented in Figure 52. The variation of the geometric contour is illustrated in Figure 53. In this two-dimensional example, the Gauss-Newton algorithm was able to substantially reduce the deviation of RP fluid dynamic parameters from the prescribed distributions leading to a substantially improved design. The number of required function evaluations is also within practical limits using current technology.

5.0 SUMMARY AND CONCLUSIONS

The objective of this research was satisfied by developing an aerodynamic optimization technique that coupled an existing Euler/Navier-Stokes solver with efficient nonlinear least-squares minimization algorithms and by successfully applying the technique to representative aerodynamic design problems. This demonstrated that the Euler/Navier-Stokes CFD simulations were reliable enough for use in coupling with Gauss-Newton-based optimization algorithms. In fact, for two examples presented, a quasi-Newton algorithm was successfully applied to determine the optimal design variables. The examples were deliberately started from poor initial designs to evaluate the capability of the design technique to converge in spite of poor initial conditions.

To date, this research has evaluated the feasibility of coupling nonlinear optimization methods with CFD. Existing Gauss-Newton and quasi-Newton optimization algorithms were employed with minimal modifications with good results obtained for several representative aerodynamic design problems. The quasi-Newton algorithm was not successful for the more aerodynamically complex examples, but was significantly more efficient when applicable. This suggests that alternating between the two algorithms may produce a more efficient optimization strategy if reliable switching criteria can be determined. Because of the complexity of the motivating application, the optimization algorithms were coupled with an Euler/Navier-Stokes CFD code, which makes the function evaluations computationally expensive. However, the same method could be coupled with a less complex CFD technique for design problems in which an Euler or Navier-Stokes simulation is not required.

The approach presented provides the designer with a potentially powerful tool to assist in many designs for which a measure of design quality (objective function) can be adequately defined. Because of the flexibility afforded by the current CFD codes, this technique can be applied to virtually any steady-state aerodynamic optimization problem for which the selected CFD code is capable of providing a reliable aerodynamic analysis. The design method is reliable in the sense that improvements to the initial design are achieved, and it is efficient in terms of minimizing the number of function evaluations required to determine the optimal design variables. For complex two-dimensional aerodynamic designs, the method requires on the order of 50 function evaluations, which is feasible with access to modern supercomputers. However, because of the computational expense caused by the multiple CFD simulations, three-dimensional applications of the technique will most likely be restricted in the near term to aerodynamic configurations such as the noted forebody simulator design for which satisfaction of the design criteria is of great importance and simple alternative design methods do not exist.

6.0 RECOMMENDATIONS

There are several areas where improvements could be made to enhance the design optimization process. One possible enhancement would be to alter the optimization strategy by combining the quasi-Newton algorithm and the Gauss-Newton algorithm in an attempt to utilize the best features of each. The strategy of alternating between the two algorithms could produce a more efficient overall optimization strategy if satisfactory switching criteria are identified. One possible criterion would be to use the value of the one-dimensional linear search parameter to indicate regions where the solution is progressing well enough to apply the quasi-Newton method. Another possible enhancement would be application of more sophisticated linear search algorithms in an effort to reduce the number of iterations required to isolate the optimal value.

Performing a design variable sensitivity study can be expensive when CFD techniques are used to perform function evaluations. However, at present, this is the recommended procedure to determine appropriate variable step sizes for use in computation of design space derivatives. A more efficient method of selecting the appropriate step sizes would significantly reduce overall computation time.

In the research presented, each CFD simulation was made fully convergent to eliminate temporal variations when computing partial derivatives with respect to each design variable. Elimination or relaxation of this constraint would significantly reduce the computer time required for each CFD simulation with a corresponding increase in efficiency of the overall design process.

BIBLIOGRAPHY

BIBLIOGRAPHY

1. Chapman, D. R. "Computational Aerodynamics Development and Outlook." AIAA Journal, Vol. 17, No. 12, December 1979, pp. 1293-1313.

2. Beale, D. K. and Collier, M. S. "Validation of a Free-jet Technique for Evaluating Inlet-Engine Compatibility." AIAA Paper 89-2325, AIAA/ASME/SAE/ASEE 25th Joint Propulsion Conference, Monterey, California, July 1989.

3. Zannetti, L. "Time Dependent Method to Solve the Inverse Problem for Internal Flows." AIAA Journal, Vol. 18, No. 7, July 1980, pp. 754-758.

4. McCormack, R. W. "The Effects of Viscosity in Hypervelocity Impact Cratering." AIAA Paper 69-354, 1969.

5. Zannetti, L. and Pandolfi, M. "Inverse Design Technique for Cascades." NASA CR 3836, November 1984.

6. Moretti, G. "The λ-scheme." Computers and Fluids, Vol. 7, No. 9, September 1979, pp. 191-205.

7. Yang, T. and Ntone, F. "Viscous Compressible Flow Direct and Inverse Computation with Illustration." NASA CR 175037, January 1986.

8. Vanderplaats, G. N. "An Efficient Algorithm for Numerical Airfoil Optimization." AIAA Paper No. 79-0079, 17th Aerospace Sciences Meeting, New Orleans, Louisiana, January 1979.

9. Barger, R. L. "Solution of Complex Nonlinear Problems by a Generalized Application of the Method of Base and Comparison Solutions With Applications to Aerodynamics Problems." NASA TP 1857, May 1981.

10. Barger, R. L. and Moitra, A. "On Minimizing the Number of Calculations in Design-by-Analysis Codes." NASA TP 2706, June 1987.

11. Pittman, J. L. "Supersonic Airfoil Optimization." Journal of Aircraft, Vol. 24, No. 12, December 1987, pp. 873-880.

12. Aidala, P. V., Davis, W. H., and Mason, W. H. "Smart Aerodynamic Optimization." AIAA Paper No. 83-1863, AIAA Applied Aerodynamics Conference, Danvers, Massachusetts, July 1983.

13. Davis, W. H. "TRO-2D A Code for Rational Transonic Aero Optimization." AIAA Paper No. 85-0425, AIAA 23rd Aerospace Sciences Meeting, Reno, Nevada, January 1985.

14. Davis, W. H. "Technique for Developing Design Tools from the Analysis Methods of Computational Aerodynamics." AIAA Journal, Vol. 18, No. 9, September 1980, pp. 1080-1087.

15. Madabhushi, R. K., Levy, R., and Pincus, S. M. "Design of Optimum Ducts Using an Efficient 3-D Viscous Computational Flow Analysis." Proceedings of the Second International Conference on Inverse Design Concepts and Optimization in Engineering Sciences ICIDES-II, October 1987, pp. 147-166.

16. Huddleston, D. H. and Mastin, C. W. "Optimization Methods Applied to Aerodynamic Design Problems in Computational Fluid Dynamics." 7th International Conference on Finite Element Methods in Flow Problems, Huntsville, Alabama, April 1989.

17. Huddleston, D. H. and Mastin, C. W. "Optimization of Aerodynamic Designs Using Computational Fluid Dynamics." AGARD Specialists' Meeting on Computational Methods for Aerodynamic Design (Inverse) and Optimization, Loen, Norway, May 1989.

18. Cooper, G. K. "Toward a General Purpose Navier-Stokes Code." Abstracts of the First World Congress on Computational Mechanics, Vol. I, Austin, Texas, September 22-26, 1986.

19. Phares, W. J., Cooper, G. K., Swafford, T. W., and Jones, R. R. "Application of Computational Fluid Dynamics to Test Facility and Experimental Design." AIAA Paper 86-1733, AIAA/ASME/SAE/ASEE 22nd Joint Propulsion Conference, Huntsville, Alabama, July 1986.

20. Huddleston, D. H., Cooper, G. K., and Phares, W. J. "A Computational Fluid Dynamics Evaluation of Test Cell Recirculation Effects on High-Bypass Turbofan Engine Surface Pressure Distributions." AIAA Paper 86-1384, AIAA/ASME/SAE/ASEE 22nd Joint Propulsion Conference, Huntsville, Alabama, July 1986.

21. Cooper, G. K. and Jordon J. "Analysis Tool for Application to Ground Testing of Highly Underexpanded Nozzles." AIAA Paper 87-2015, AIAA/ASME/SAE/ASEE 23rd Joint Propulsion Conference, San Diego, California, July 1987.

22. Soni, B. K. "Two- and Three-Dimensional Grid Generation for Internal Flow Applications of Computational Fluid Dynamics." AIAA Paper 85-1526, AIAA 7th Computational Fluid Dynamics Conference, Cincinnati, Ohio, 1985.

23. Scales, L. E. Introduction to Non-Linear Optimization. Springer-Verlag, New York, 1985, pp. 110-115, 125-127.

24. Hartley, H. O. "The Modified Gauss-Newton Method for the Fitting of Nonlinear Regression Functions by Least Squares." Technometrics, Vol. 3, May 1961, pp. 269-280.

25. Broyden, C. G. "A Class of Methods for Solving Nonlinear Simultaneous Equations." Mathematics of Computation, Vol. 19, 1965, pp. 577-593.

26. Faux, I. D. and Pratt, M. J. Computational Geometry for Design and Manufacture. Ellis Horwood Limited, Chichester, West Sussex, England, 1985, pp. 132-134, 218, 293.

27. Gill, P. E. "The Implementation of Two Modified Newton Algorithms for Unconstrained Optimization." Report NAC24, NPL, Teddington, England, August 1972.

28. Jameson, A. and Mavriplis, D. "Finite Volume Solution of the Two-Dimensional Euler Equations on a Regular Triangular Mesh." AIAA Journal, Vol. 24, No. 4, April 1986, pp. 611-618.

APPENDIXES

APPENDIX A

FIGURES

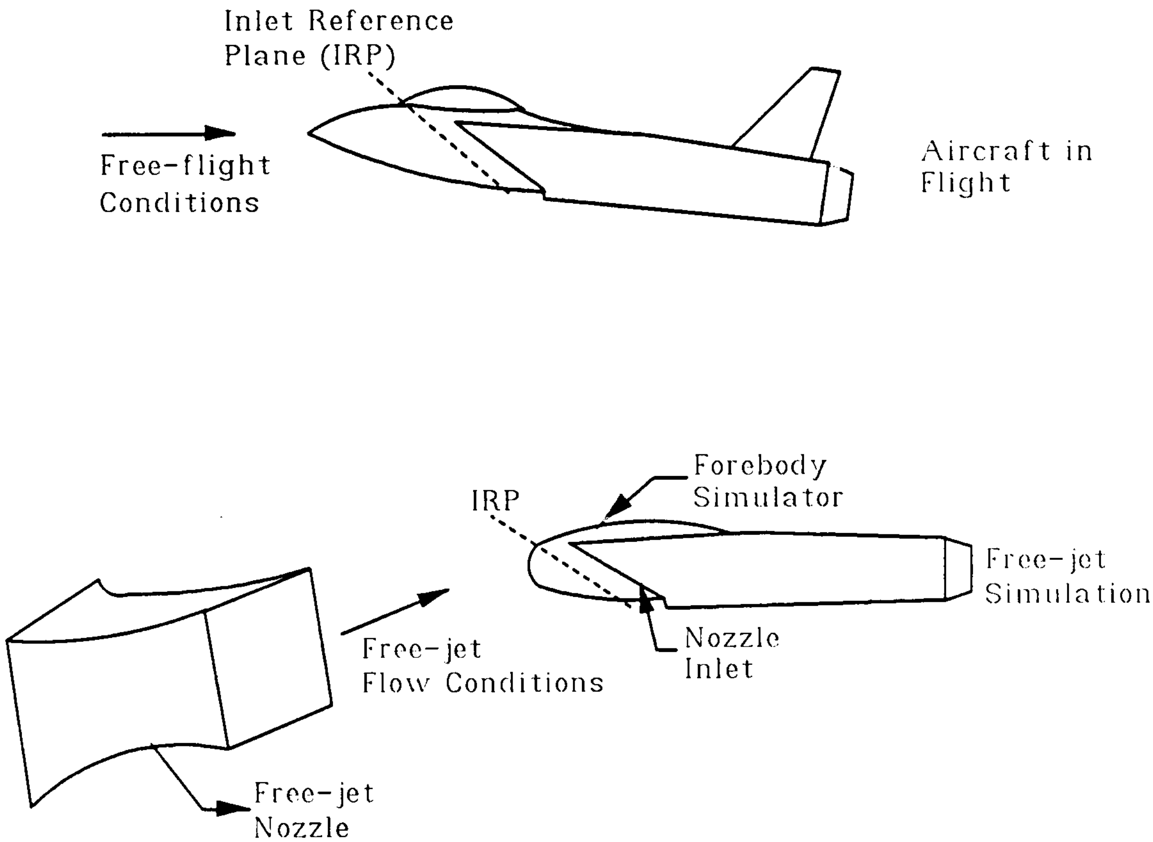

Figure 1. Generic free-jet engine/inlet compatibility test configuration.

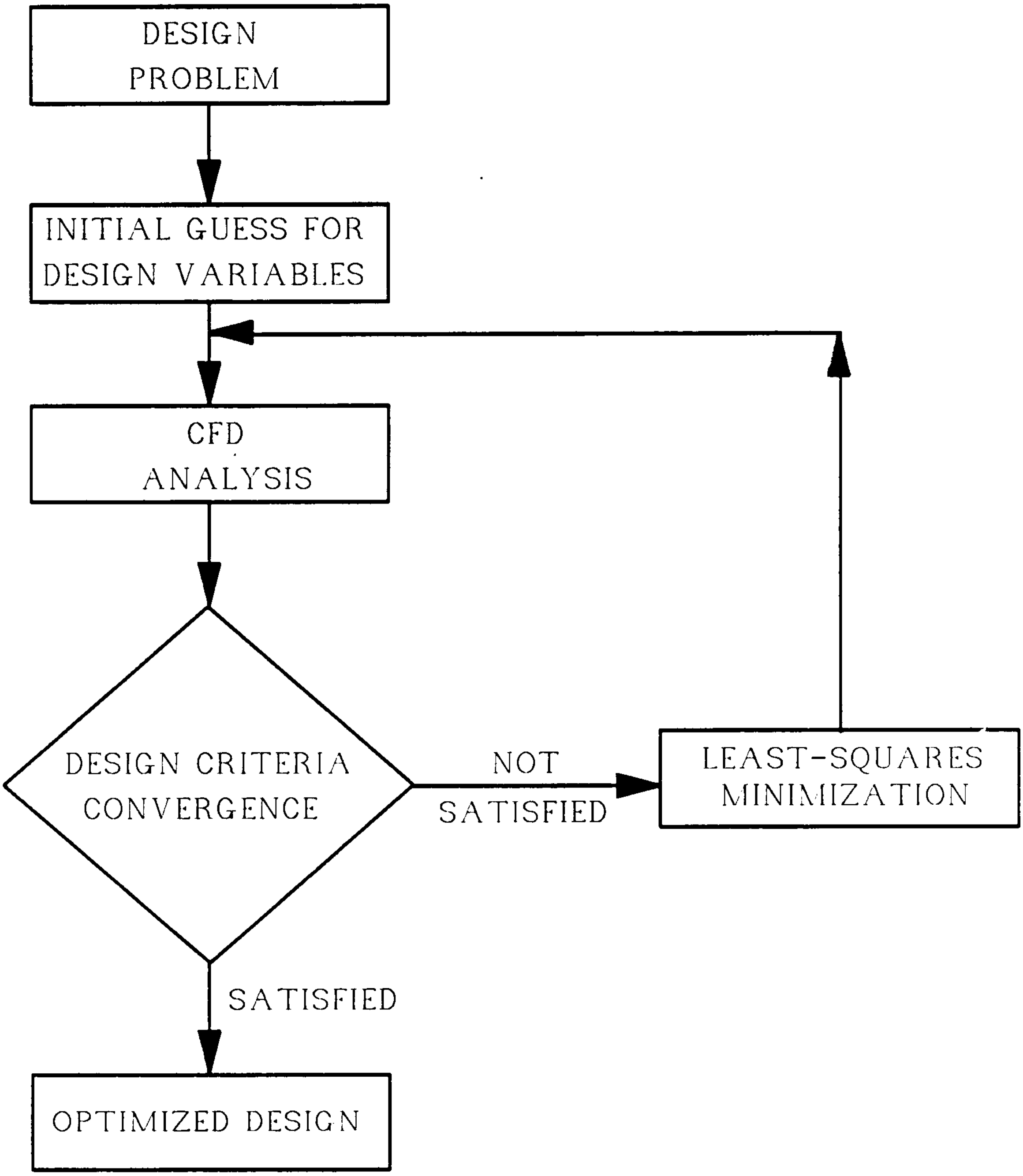

Figure 2. Design optimization strategy.

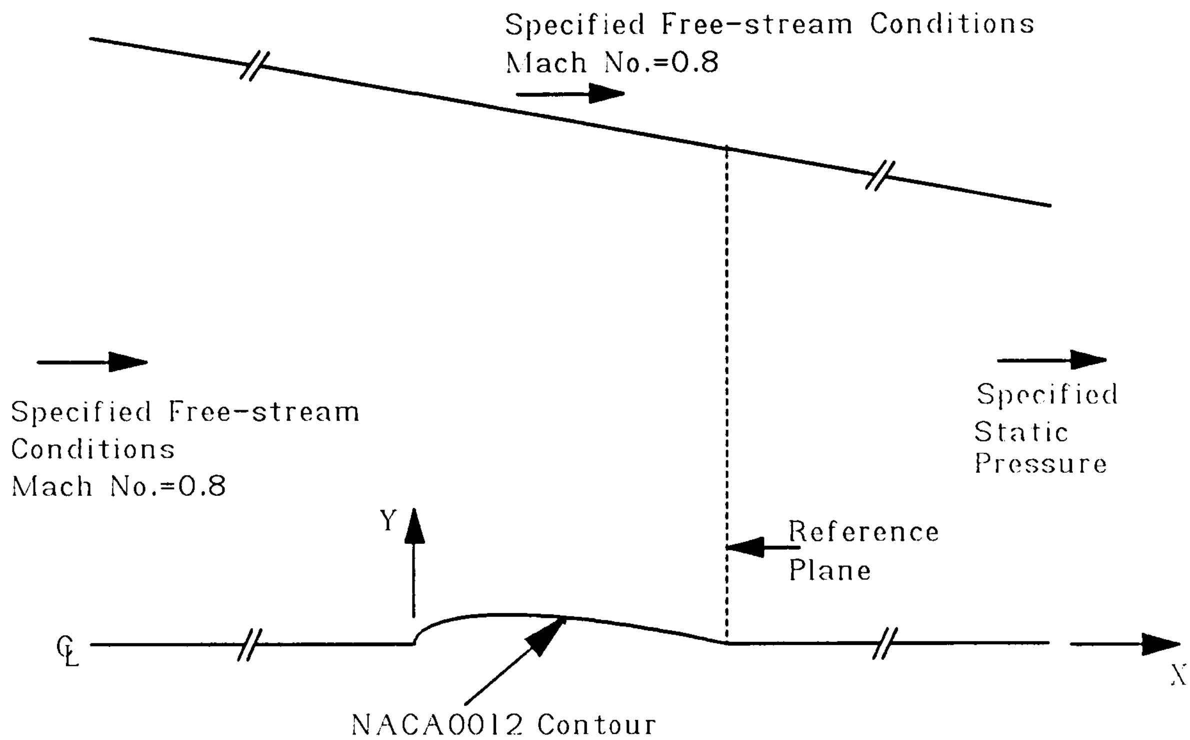

Figure 3. Inviscid airfoil optimization.

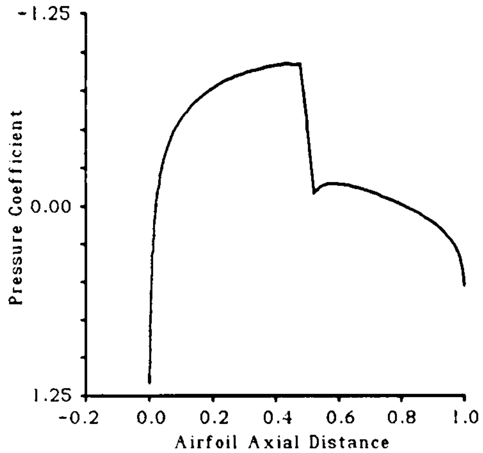

Figure 4. Inviscid airfoil surface pressure distribution.

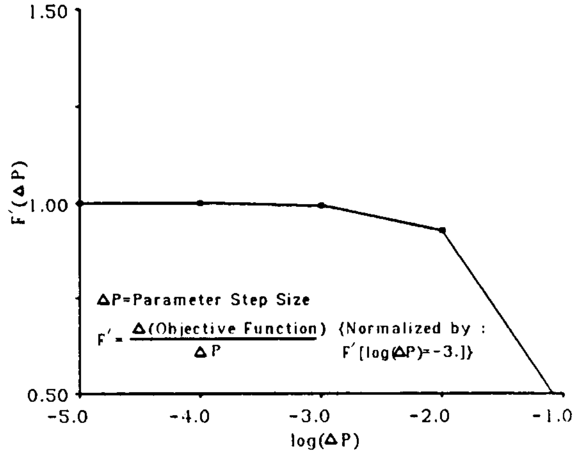

Figure 5. Inviscid airfoil derivative sensitivity.

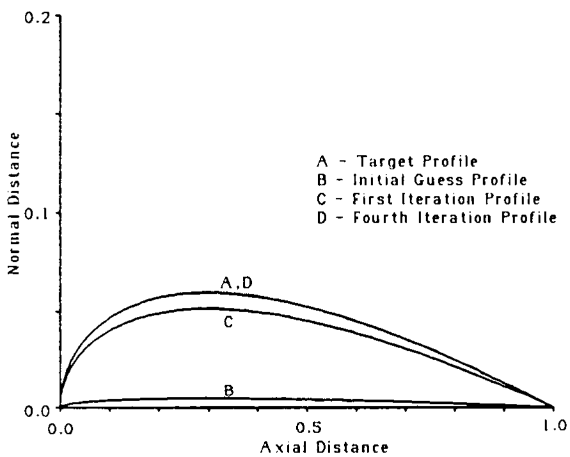

Figure 6. Inviscid airfoil contour variation.

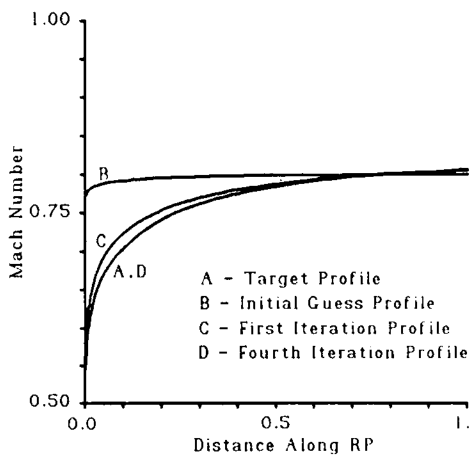

Figure 7. Inviscid airfoil reference plane Mach number profiles.

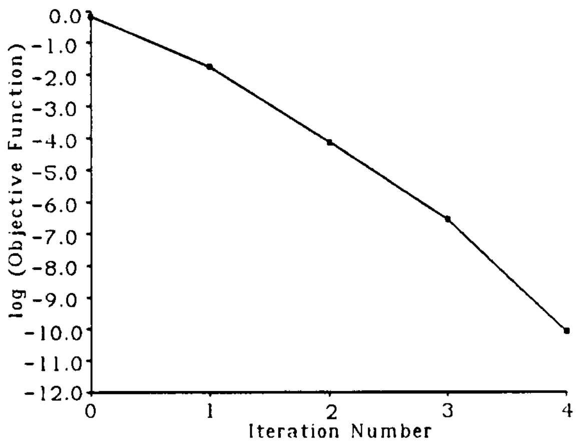

Figure 8. Inviscid airfoil objective function reduction.

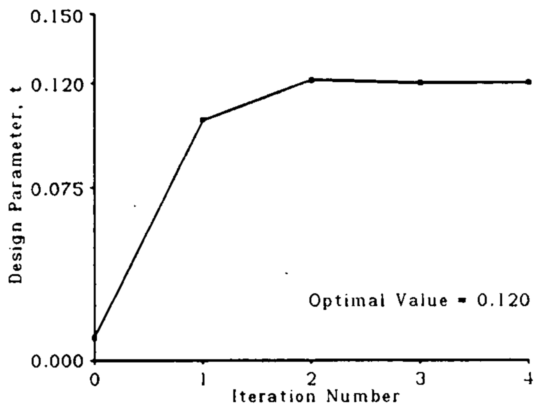

Figure 9. Inviscid airfoil design parameter convergence.

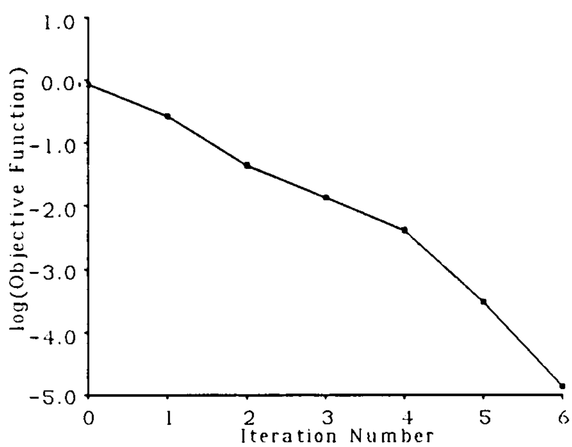

Figure 10. Inviscid airfoil objective function reduction for specified P(x).

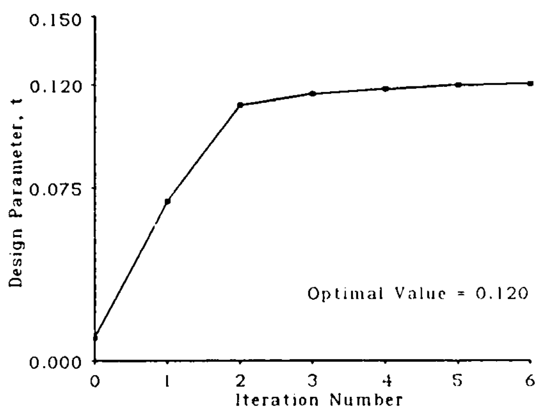

Figure 11. Inviscid airfoil design parameter convergence for specified P(x).

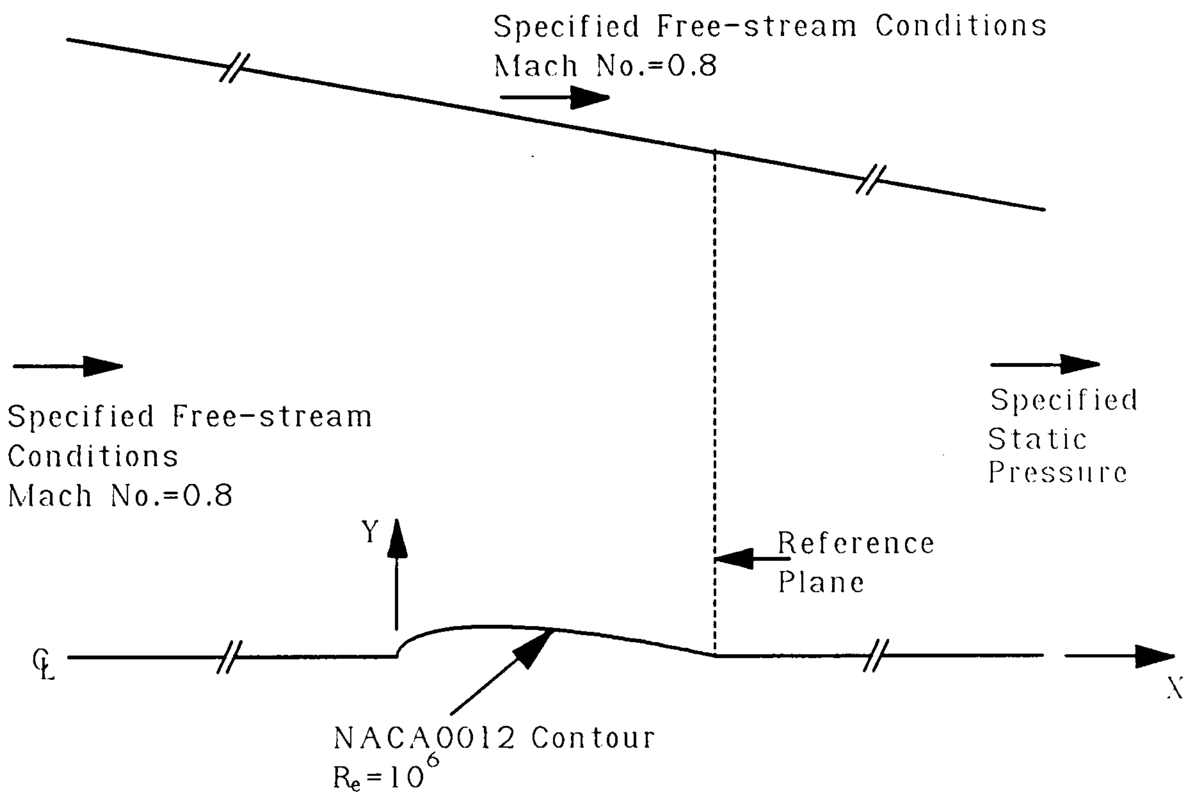

Figure 12. Viscous airfoil optimization.

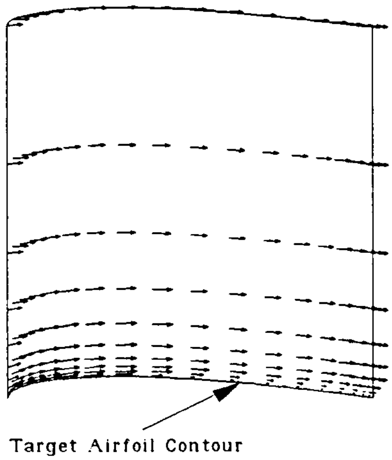

Figure 13. Viscous airfoil target velocity field.

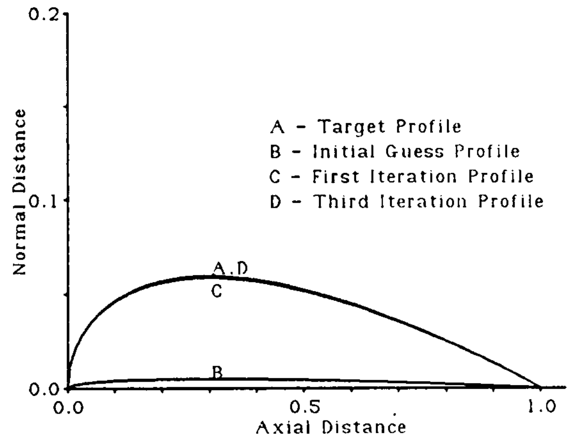

Figure 14. Viscous airfoil contour variation.

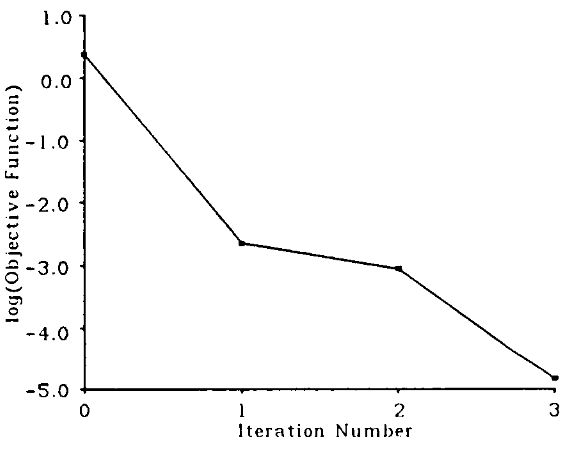

Figure 15. Viscous airfoil objective function reduction.

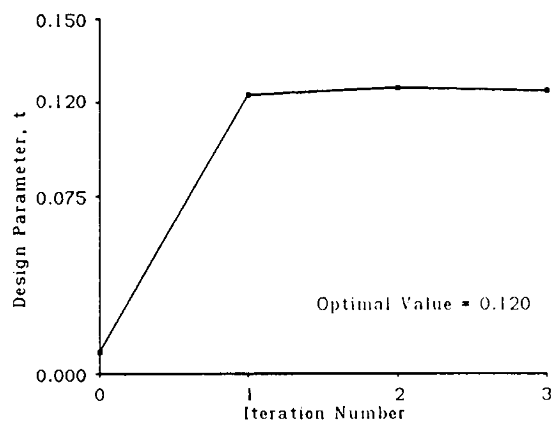

Figure 16. Viscous airfoil design parameter convergence.

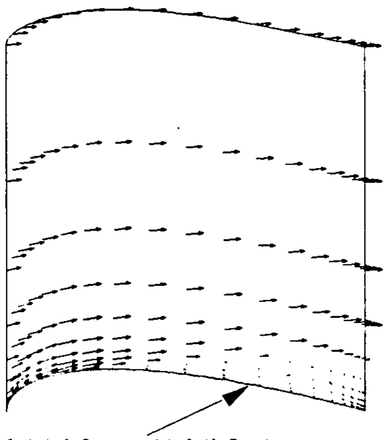

Figure 17. Separated viscous airfoil initial guess velocity field.

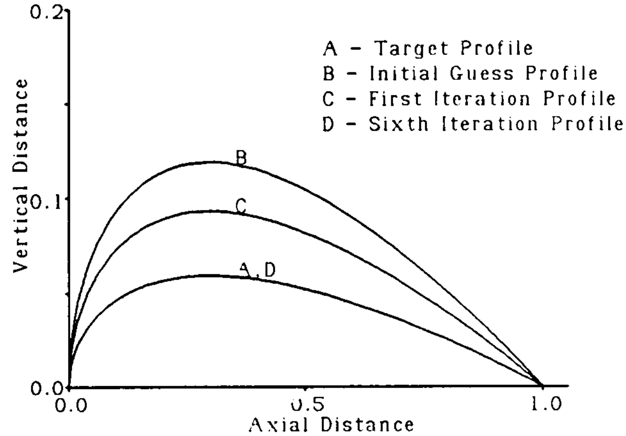

Figure 18. Separated viscous airfoil contour variation.

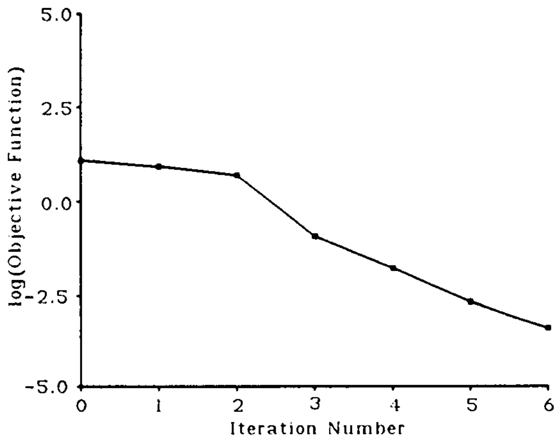

Figure 19. Separated viscous airfoil objective function reduction.

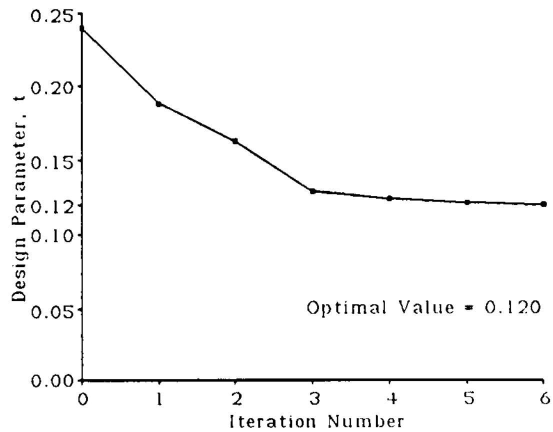

Figure 20. Separated viscous airfoil design parameter convergence.

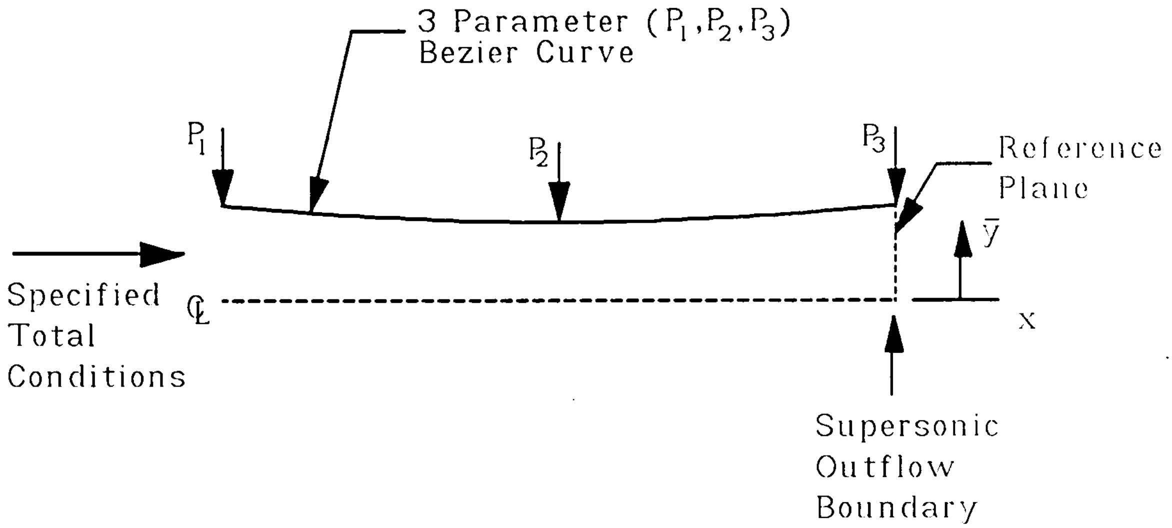

Figure 21. Planar convergent/divergent nozzle optimization.

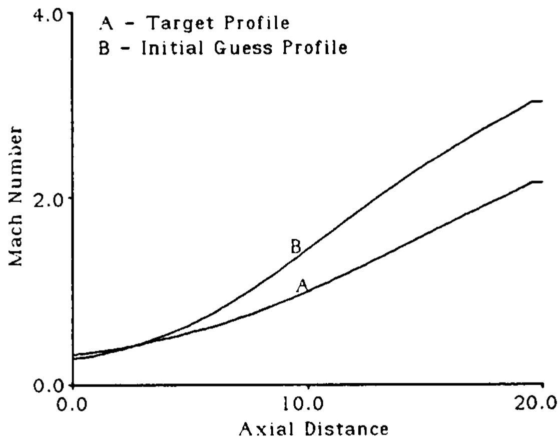

Figure 22. Planar convergent/divergent nozzle centerline Mach number distribution.

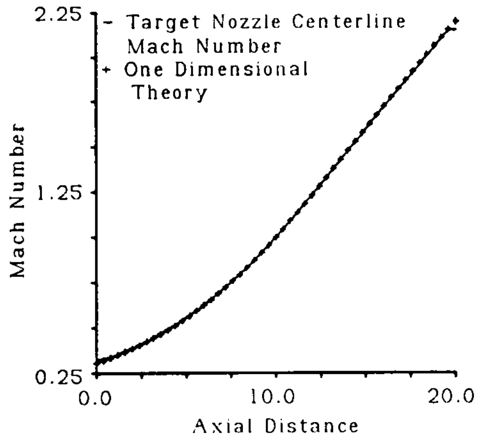

Figure 23. Planar convergent/divergent nozzle centerline Mach number comparison to one-dimensional theory.

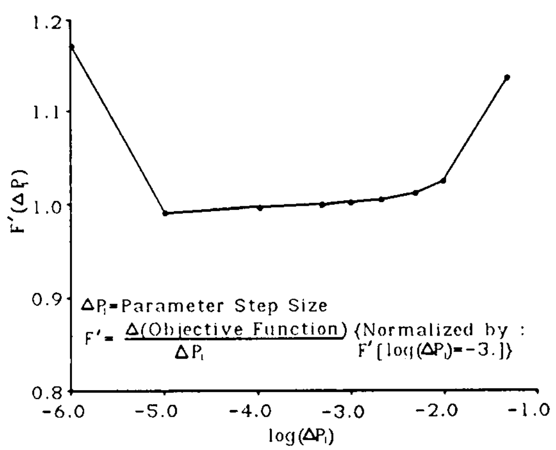

Figure 24. Planar convergent/divergent nozzle objective function derivative sensitivity.

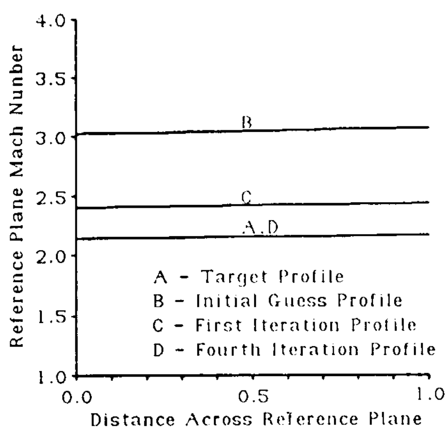

Figure 25. Planar convergent/divergent nozzle RP Mach number profiles.

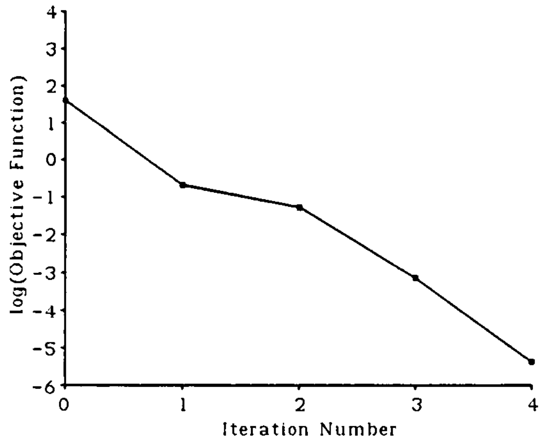

Figure 26. Planar convergent/divergent nozzle objective function reduction.

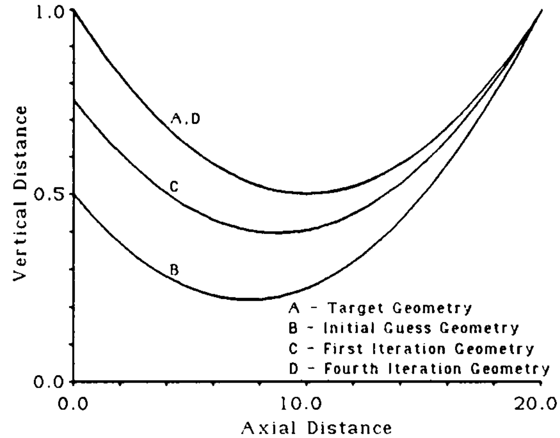

Figure 27. Planar convergent/divergent nozzle wall contour variation.

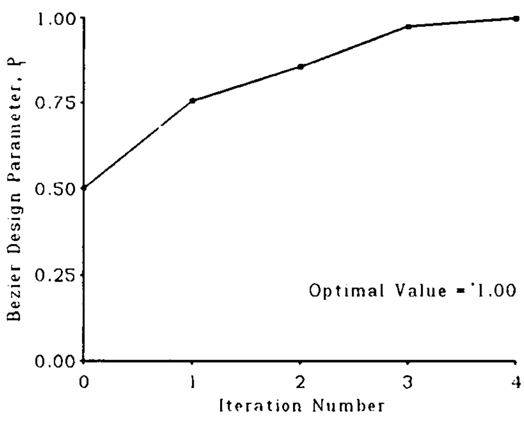

Figure 28. Planar convergent/divergent nozzle Bezier design parameter, P_1, convergence.

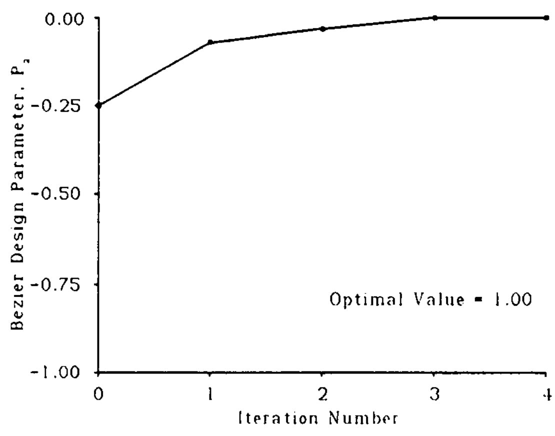

Figure 29. Planar convergent/divergent nozzle Bezier design parameter, P_2, convergence.

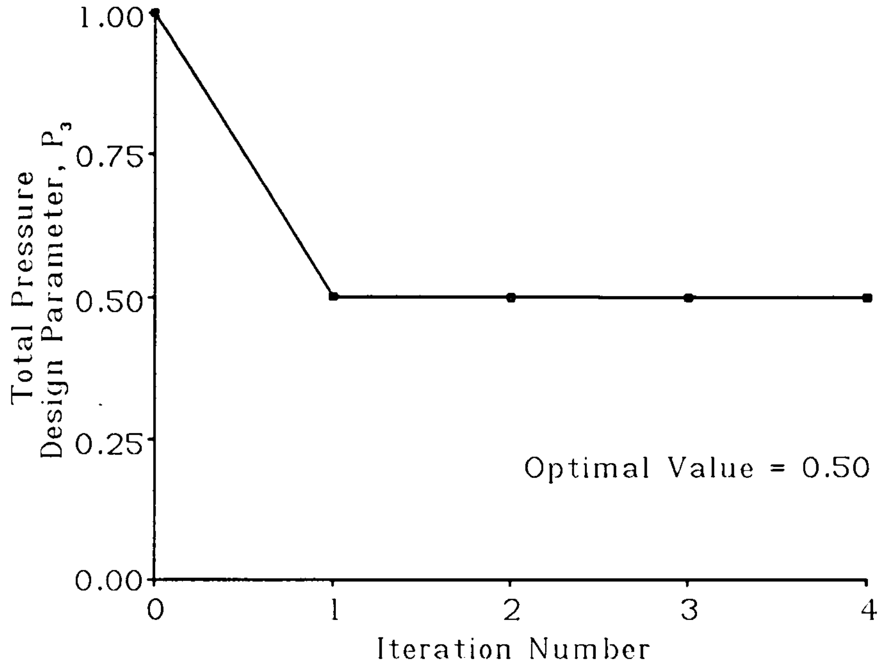

Figure 30. Planar convergent/divergent nozzle total pressure design parameter, P_3, convergence.

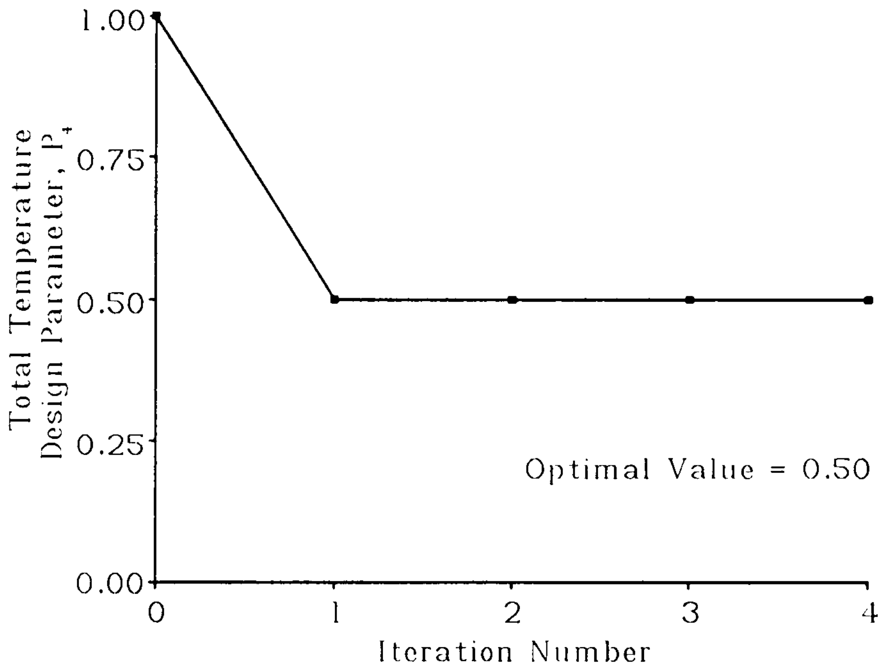

Figure 31. Planar convergent/divergent nozzle total temperature design parameter, P_4, convergence.

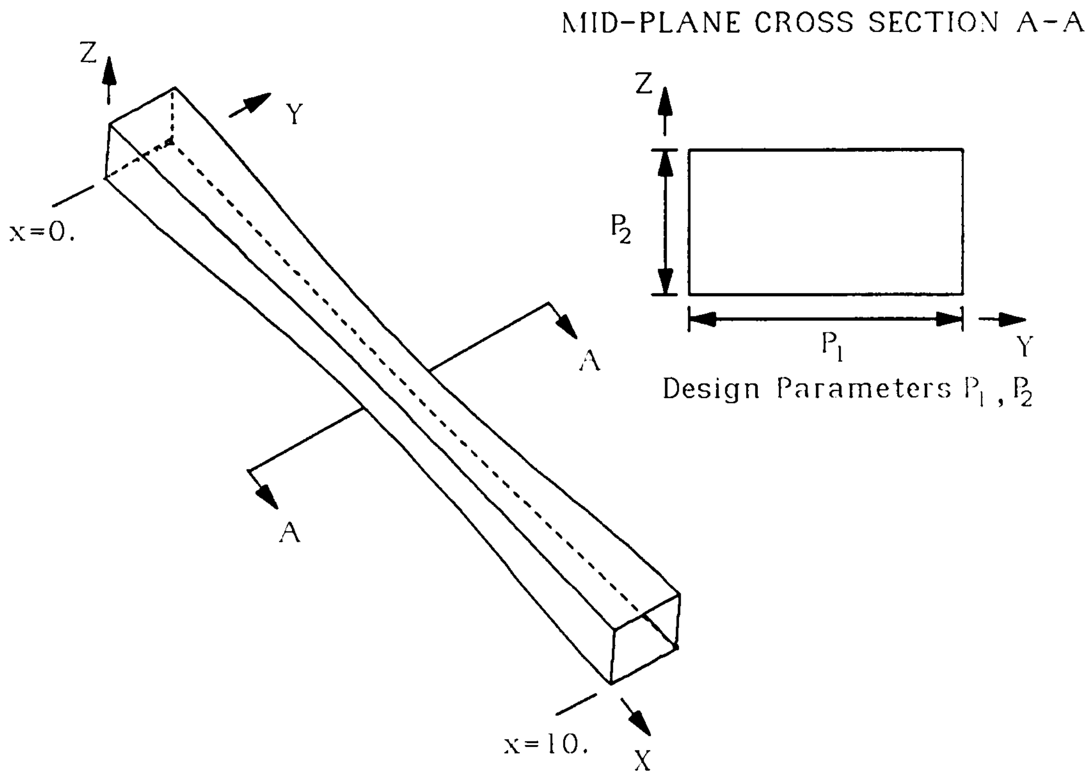

Figure 32. 3D convergent/divergent nozzle optimization.

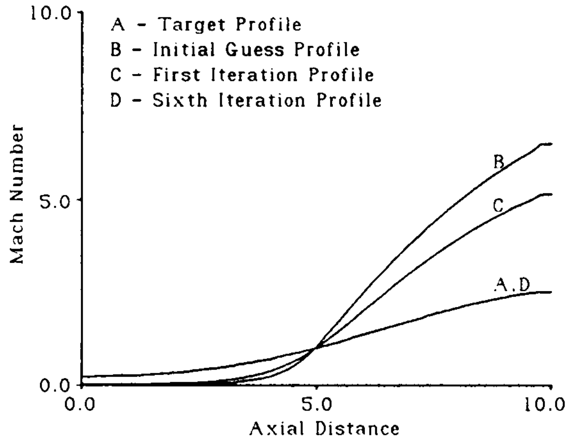

Figure 33. 3D convergent/divergent nozzle centerline Mach number distribution comparison.

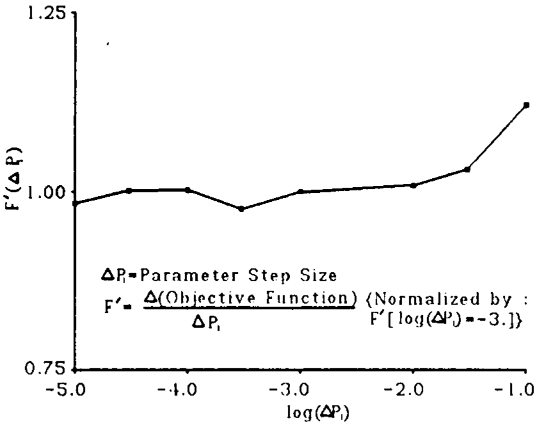

Figure 34. 3D convergent/divergent nozzle derivative sensitivity.

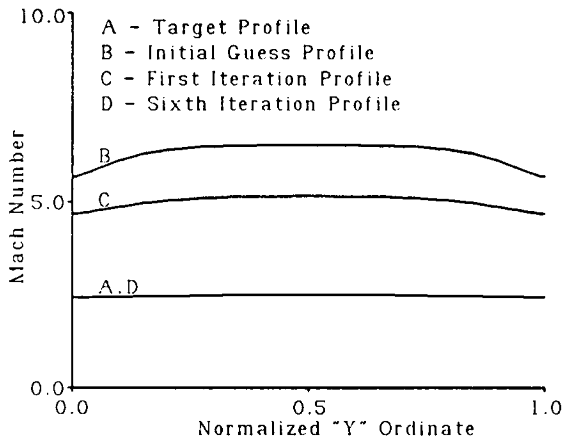

Figure 35. 3D convergent/divergent nozzle RP Mach number variation (Z=0.0).

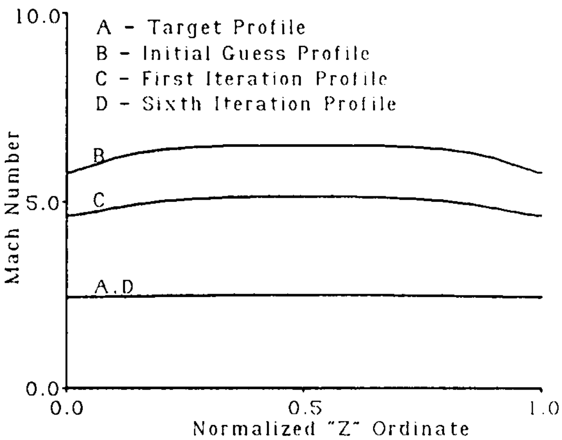

Figure 36. 3D convergent/divergent nozzle RP Mach number variation (Y=0.0).

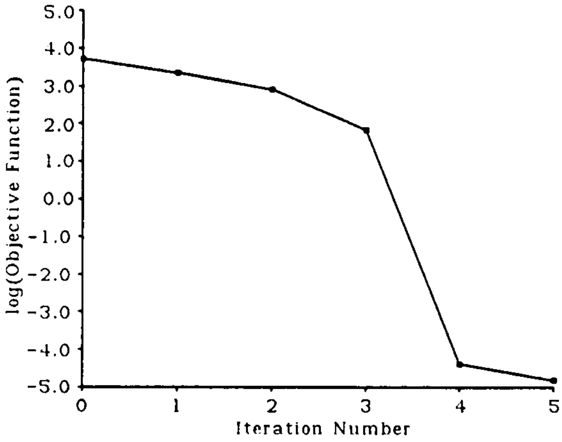

Figure 37. 3D convergent/divergent nozzle objective function reduction.

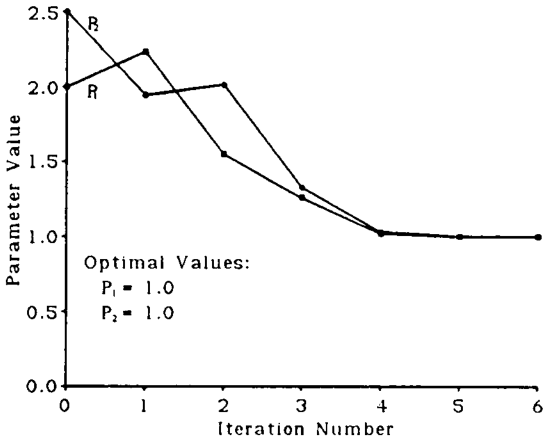

Figure 38. 3D convergent/divergent nozzle design parameter convergence.

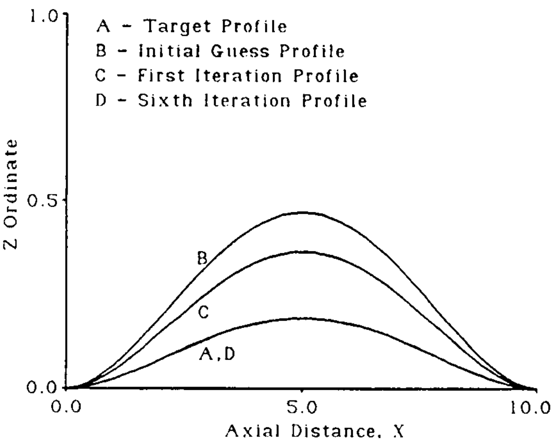

Figure 39. 3D convergent/divergent nozzle wall contour convergence for constant "Y" plane.

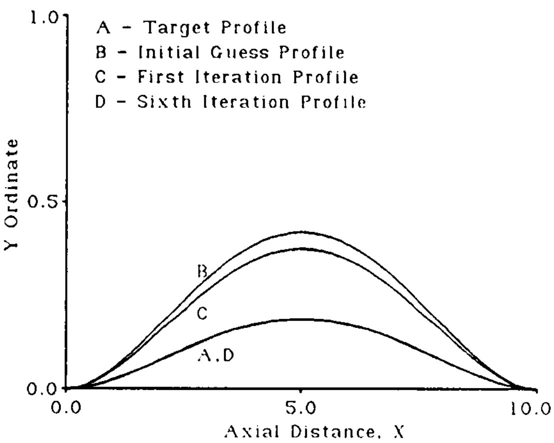

Figure 40. 3D convergent/divergent nozzle wall contour convergence for constant "Z" plane.

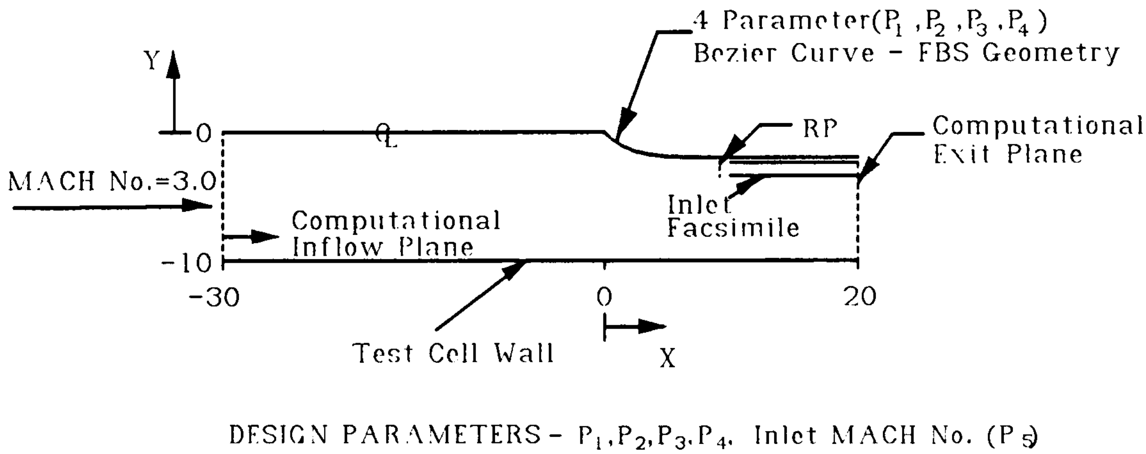

Figure 41. Planar supersonic forebody simulator optimization.

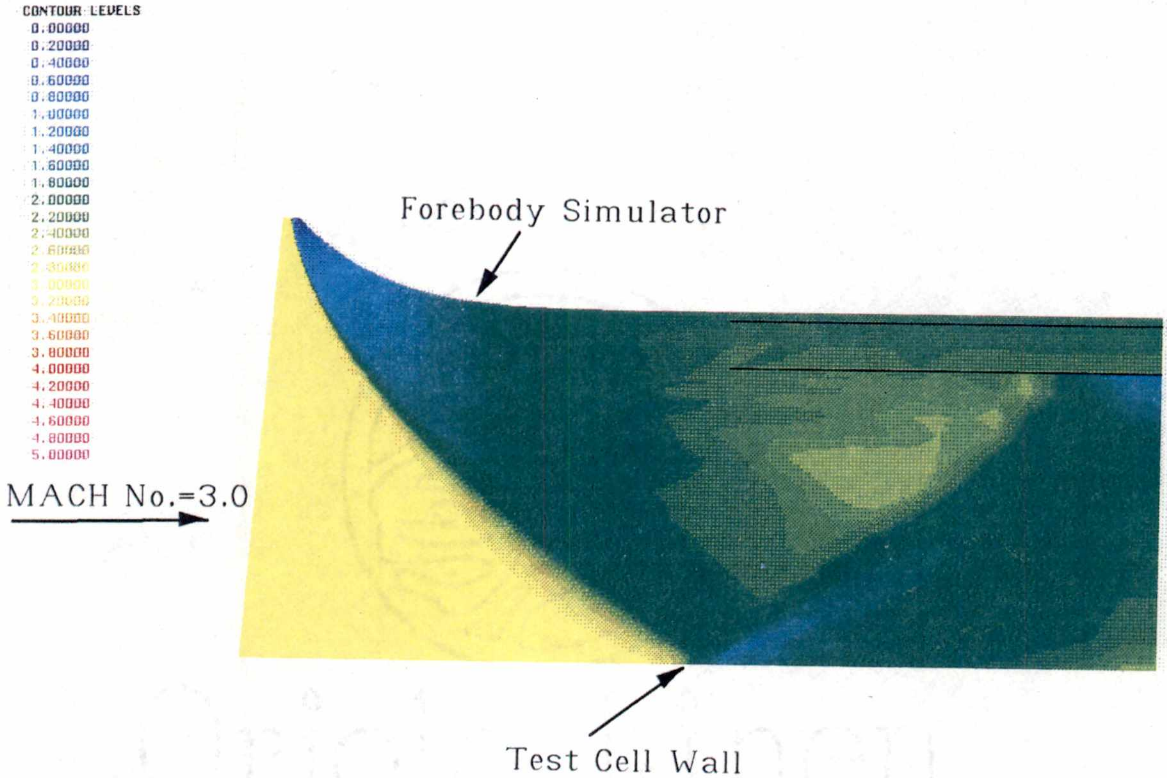

Figure 42. Target design Mach contours in the forebody simulator/inlet region.

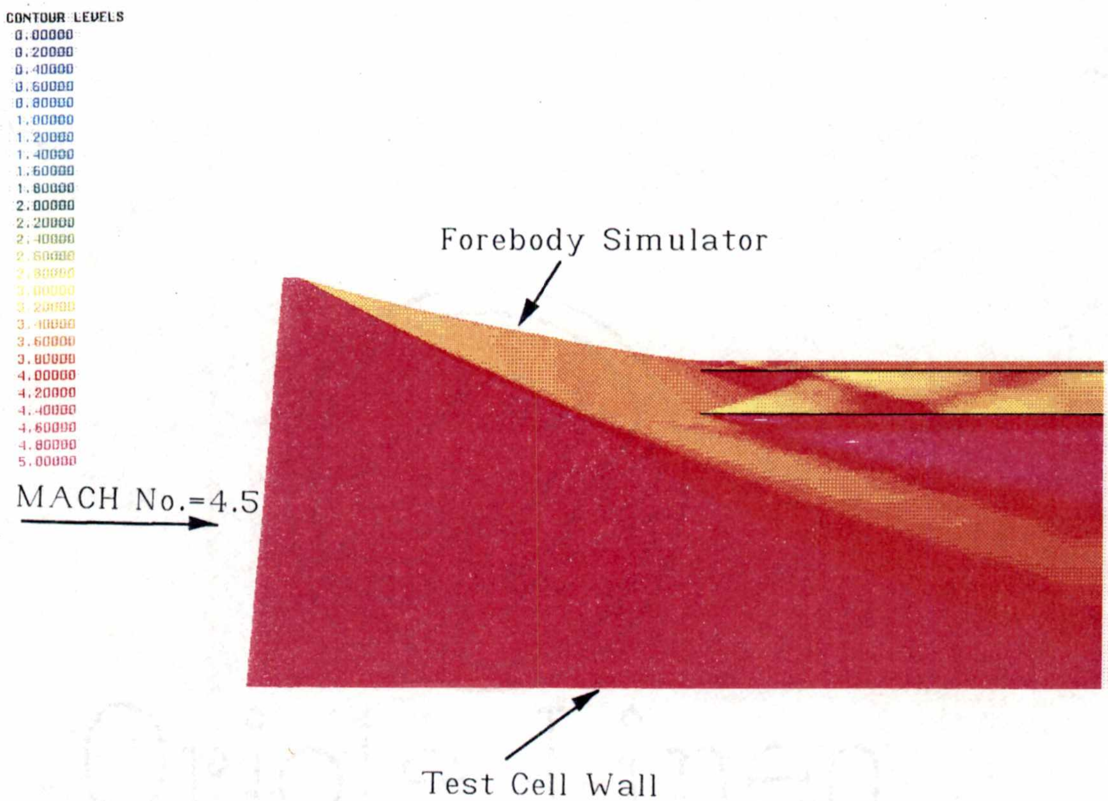

Figure 43. Initial guess Mach contours in the forebody simulator/inlet region.

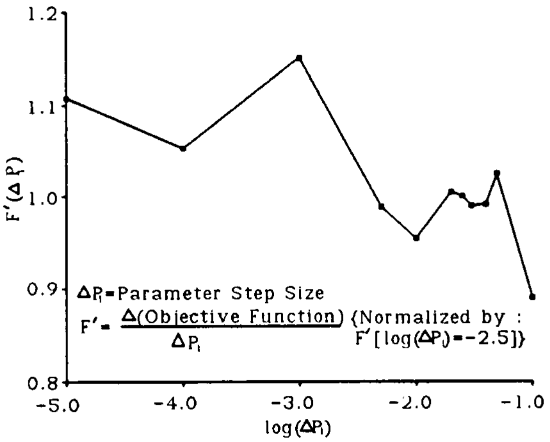

Figure 44. Planar supersonic forebody simulator derivative sensitivity.

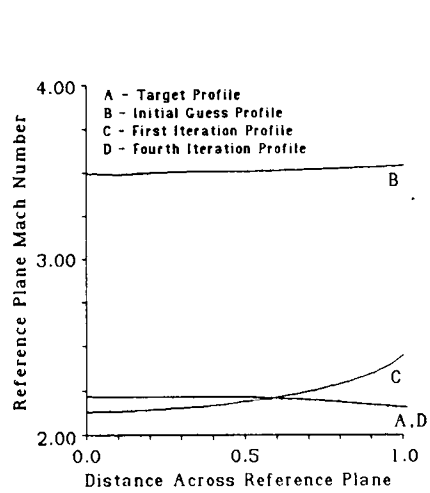

Figure 45. Planar supersonic forebody simulator RP Mach number profiles.

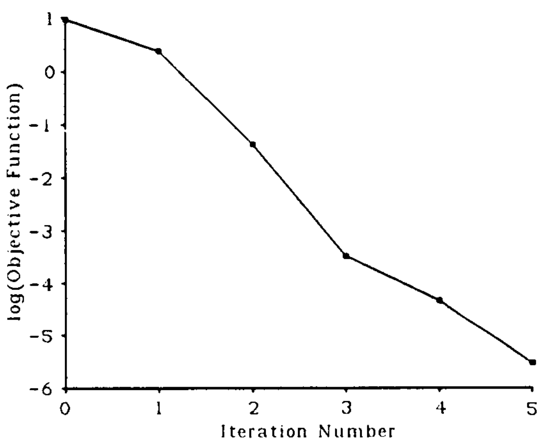

Figure 46. Planar supersonic forebody simulator objective function reduction.

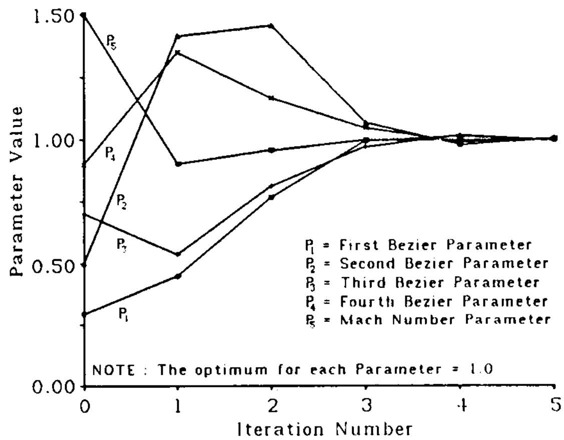

Figure 47. Planar supersonic forebody simulator design parameter convergence.

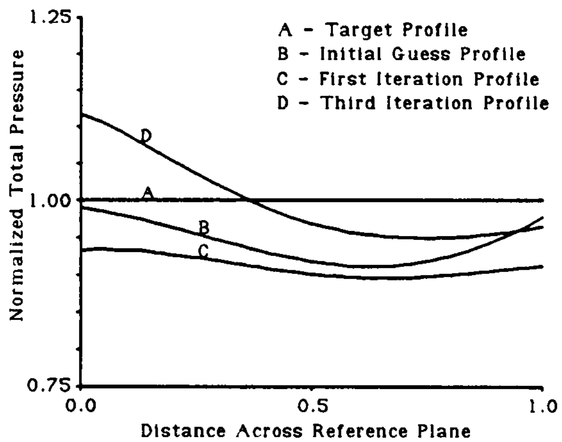

Figure 48. Comparison of the total pressure component of the objective function for a shortened forebody simulator.

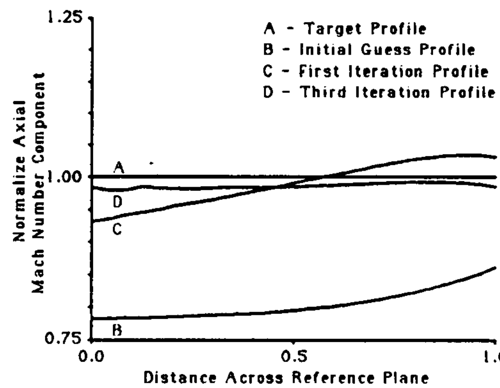

Figure 49. Comparison of the axial Mach number component of the objective function for a shortened forebody simulator.

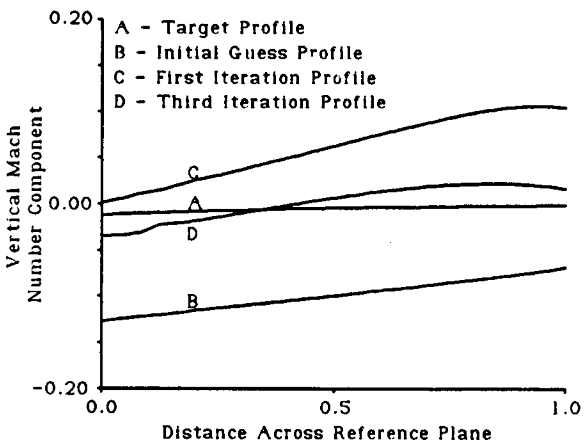

Figure 50. Comparison of the vertical Mach number component of the objective function for a shortened forebody simulator.

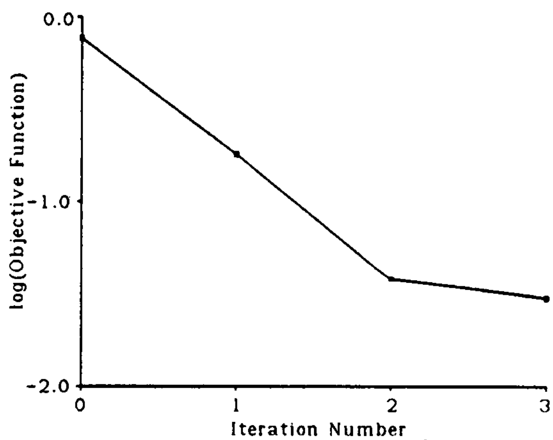

Figure 51. Shortened supersonic forebody simulator objective function reduction.

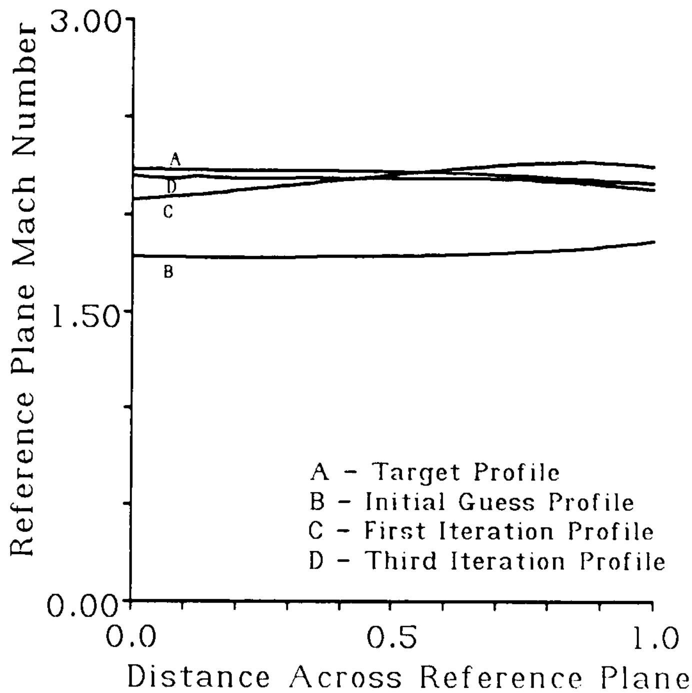

Figure 52. Shortened supersonic forebody simulator RP Mach number profiles.

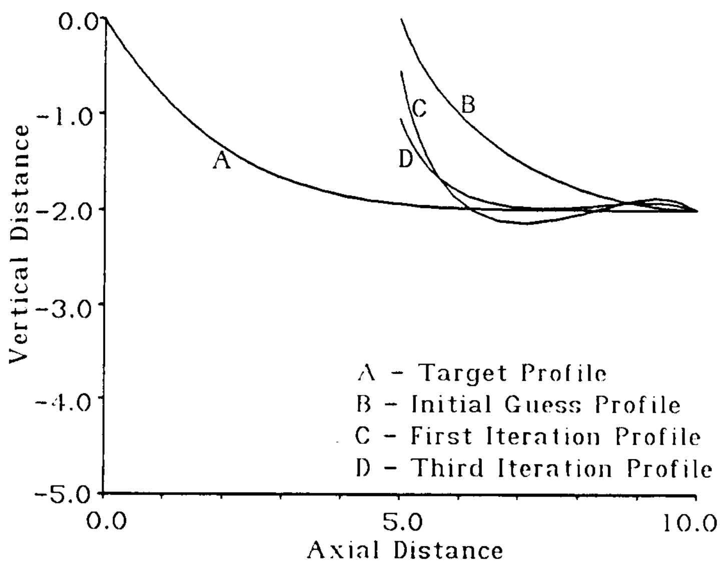

Figure 53. Shortened supersonic forebody simulator variation in variable geometry.

APPENDIX B

GAUSS-NEWTON ALGORITHM

To formulate the nonlinear least-squares minimization, let the residuals $r_i(P_1,\ldots,P_M)$, $i=1,2,\ldots,N$, be functions of the M design parameters, $\underline{P}$. To minimize r_i, in the least-squares sense, values for the parameters, $\underline{P}$, are found which minimizes

$$F(\underline{P}) = \sum_{i=1}^{N} \left\{ y_i - f_i(\underline{P}) \right\}^2 = \sum_{i=1}^{N} \left\{ r_i(\underline{P}) \right\}^2 \tag{B.1}$$

where y_i denotes the N specified reference plane quantities, and f_i denotes the computed M quantities for the associated design parameters, $\underline{P}$.

The Gauss-Newton minimization algorithm is derived by first substituting a Taylor series expansion about $\underline{P}^0$ into (B.1) for $r_i(\underline{P})$. This yields

$$F(\underline{P}) \sim \sum_{i=1}^{N} \left\{ r_i\left(\underline{P}^0\right) + \sum_{j=1}^{M} \frac{\partial r_i\left(\underline{P}^0\right)}{\partial P_j} \Delta P_j \right\}^2 \tag{B.2}$$

with ΔP_j defined as the j^{th} component of the vector

$$\Delta \underline{P} = \underline{P} - \underline{P}^0 \tag{B.3}$$

Minimizing (B.2) requires

$$\frac{\partial F(\underline{P})}{\partial P_k} = 0 \tag{B.4}$$

for each k. Applying condition (B.4) to equation (B.2) and neglecting higher order terms yields the following system of equations:

$$2\sum_{i=1}^{N}\{r_i(\underline{P}^0) + \sum_{j=1}^{M}\frac{\partial r_i(\underline{P}^0)}{\partial P_j}\Delta P_j\}\frac{\partial r_i(\underline{P}^0)}{\partial P_k} = 0 \tag{B.5}$$

for k=1,2,3,...,M. Rearranging (B.5)

$$\sum_{i=1}^{N}\left\{\sum_{j=1}^{M}\frac{\partial r_i(\underline{P}^0)}{\partial P_j}\Delta P_j\right\}\frac{\partial r_i(\underline{P}^0)}{\partial P_k} = -\sum_{i=1}^{N}\left\{r_i(\underline{P}^0)\frac{\partial r_i(\underline{P}^0)}{\partial P_k}\right\} \tag{B.6}$$

Defining J as the Jacobian matrix of the residual vector, $\underline{R}$, with respect to the parameter vector, $\underline{P}$, allows the M equations defined by Eq. (B.6) to be written more concisely in vector notation as

$$J^T J \Delta \underline{P} = -J^T \underline{R} \tag{B.7}$$

This M-by-M system of equations is then solved to determine the parameter corrections at each iteration.

APPENDIX C

BROYDEN'S JACOBIAN UPDATE FORMULA

Application of the Gauss-Newton optimization algorithm requires solution of the system of equations,

$$J^T J \Delta \underline{P} = -J^T \underline{R} \tag{C.1}$$

where $\underline{R}$ denotes the residual vector of length N, $\underline{P}$ denotes the parameter vector of length M, $\Delta\underline{P}$ denotes the computed change in parameters, and J denotes the Jacobian matrix of $\underline{R}$ with respect to $\underline{P}$. Equation (C.1) then determines a search vector, $\Delta\underline{P}$, and a linear search can be carried out such that

$$\underline{P}_{k+1} = \underline{P}_k + \nu \Delta \underline{P}_k \tag{C.2}$$

where ν is selected to reduce the norm of $\underline{R}_{k+1}$ sufficiently below the norm of $\underline{R}_k$. Eliminating the linear search is equivalent to specifying $\nu = 1$ in Eq. (C.2).

A quasi-Newton method is derived by assuming at the k^{th} iteration a current design point, $\underline{P}_k$, and an approximation, B_k, to J_k has been obtained. The Jacobian initial value, B_0, can be computed by a finite difference approximation. The first-order Taylor series expansion of $\underline{R}_{k+1}$ gives

$$\underline{R}_{k+1} = \underline{R}_k + J_k \Delta \underline{P}_k \tag{C.3}$$

or in terms of the Jacobian approximation, B_k,

$$B_k \Delta \underline{P}_k = \Delta \underline{R}_k \qquad \text{(C.4)}$$

A method is sought to approximate B_{k+1} without reapplying a finite difference representation. The method introduced by Broyden [27 and 29], requires that B_{k+1} satisfy the quasi-Newton condition,

$$B_{k+1} \Delta \underline{P}_k = \Delta \underline{R}_k \qquad \text{(C.5)}$$

which provides N equations for the N*M unknown elements of B_{k+1} in Eq. (C.5). This is motivated by examining the behavior when $\underline{R}$ is linear. For linear $\underline{R}$ Eq. (C.5) constrains B_{k+1} to hold exact derivative information in the direction of $\Delta \underline{P}_k$. This is apparent from Eq. (C.3), which is exact for linear $\underline{R}$. The additional N*(M-1) equations are obtained by requiring the change in $\underline{R}$ predicted by B_{k+1} in directions $\underline{q}_i$, orthogonal to $\Delta \underline{P}_k$, to be the same as would be predicted by B_k. Symbolically, that provides

$$B_{k+1} \underline{q}_i = B_k \underline{q}_i \qquad \text{(C.6)}$$

where

$$\Delta \underline{P}_k^T \underline{q}_i = 0 \qquad \text{(C.7)}$$

for each of the M-1 directions, $\underline{q}_i$. Define Q to be a matrix of vectors such that

$$Q = (\ \Delta \underline{P}_k \quad \underline{q}_1 \quad \underline{q}_2 \quad \cdots \quad \underline{q}_{(M-1)}) \qquad \text{(C.8)}$$

For convenience select the length of $\underline{q}_i$ as

$$\underline{q}_i^T \underline{q}_i = \Delta \underline{P}_k^T \Delta \underline{P}_k \tag{C.9}$$

Now

$$Q^T Q = \left(\Delta \underline{P}_k^T \Delta \underline{P}_k \right) I \tag{C.10}$$

or

$$Q^T = \left(\Delta \underline{P}_k^T \Delta \underline{P}_k \right) Q^{-1} \tag{C.11}$$

which yields

$$Q^{-1} = \frac{Q^T}{\Delta \underline{P}_k^T \Delta \underline{P}_k} \tag{C.12}$$

Combining Eq. (C.8) with Eq. (C.6) gives

$$B_{k+1} Q = B_k Q + \left(B_{k+1} \Delta \underline{P}_k - B_k \Delta \underline{P}_k \right) \underline{M} \tag{C.13}$$

where

$$\underline{M} = (1 \quad 0 \quad 0 \quad \ldots \quad 0) \tag{C.14}$$

Combining Eq. (C.5) with Eq. (C.13) gives

$$B_{k+1} Q = B_k Q + \left(\Delta \underline{R}_k - B_k \Delta \underline{P}_k \right) \underline{M} \tag{C.15}$$

Post multiplying by Q^{-1} gives

$$B_{k+1} = B_k + \left(\Delta \underline{R}_k - B_k \Delta \underline{P}_k \right) \underline{M} Q^{-1} \tag{C.16}$$

Substituting from Eq. (C.12) gives

$$B_{k+1} = B_k + \frac{\left(\Delta \underline{R}_k - B_k \Delta \underline{P}_k \right) \underline{M} Q^T}{\Delta \underline{P}_k^T \Delta \underline{P}_k} \tag{C.17}$$

which upon simplification gives

$$B_{k+1} = B_k + \frac{\left(\Delta \underline{R}_k - B_k \Delta \underline{P}_k\right) \Delta \underline{P}_k^T}{\Delta \underline{P}_k^T \Delta \underline{P}_k} \tag{C.18}$$

APPENDIX D

QUADRATIC INTERPOLATION LINEAR SEARCH

Following Hartley [28], let F_0 denote the objective function value for the initial value of the solution vector, $\underline{P}^0$, of a Gauss-Newton or quasi-Newton iteration. Let F_1 denote the objective function value at the updated value of the solution vector, $\underline{P}^1$, where $\underline{P}^1$ is given by

$$\underline{P}^1 = \underline{P}^0 + \Delta\underline{P} \tag{D.1}$$

with $\Delta\underline{P}$ denoting the computed correction to the solution vector for the optimization iteration. Let ν define a variable such that $\nu=0$ at $\underline{P}^0$ and $\nu=1$ at $\underline{P}^1$. The objective function can now be approximated in the interval (0,1) by an interpolation function with the optimization value analytically determined. In particular, if the objective function is evaluated at $\nu=m$, within the interval, then $F(\underline{P}^0+\nu\Delta\underline{P})$ can be approximated by a quadratic function of the form

$$f(\nu) = p\nu^2 + q\nu + r \tag{D.2}$$

If F_m satisfies the criterion

$$F_m < F_0 \tag{D.3}$$

and

$$F_m < F_1 \tag{D.4}$$

then a minimum of $f(\nu)$ must exist in the interval(0,1). Differentiating Eq. (D.2) with respect to ν and setting the result equal to zero yields

$$\nu^* = -\frac{q}{2p} \tag{D.5}$$

with ν^* denoting the location of the minimum of $F(\nu)$ in the interval. The system of equations

$$\begin{pmatrix} 0 & 0 & 1 \\ 1 & 1 & 1 \\ m^2 & m & 1 \end{pmatrix} \begin{pmatrix} p \\ q \\ r \end{pmatrix} = \begin{pmatrix} F_0 \\ F_1 \\ F_m \end{pmatrix} \tag{D.6}$$

is solved to determine the coefficients p, q, and r of the quadratic. Substituting these coefficients into Eq. (D.5) yields

$$\nu^* = \frac{1}{2}\frac{(1-m^2)F_0 + m^2 F_1 - F_m}{(1-m)F_0 + m F_1 - F_m} \tag{D.7}$$

The functional value $f(\nu^*)$ should then be a better approximation to the minimum than F_1, which resulted from the optimization algorithm. Because of the expense of function evaluations within this research, the described line search was not applied unless the optimization algorithm failed to produce a reduction in functional value as

$$F_1 < F_0 \tag{D.8}$$

A similar quadratic line search method can be derived for the interval by using F_0, F_1, and the $f'(0)$. Since $f'(0)$ is computed to implement the optimization algorithm, this approach eliminates the need for the evaluation of F_m. This implementation was not evaluated herein.

APPENDIX E

ALGEBRAIC TEST FUNCTIONS

I. Rosenbrock Function

This function possesses a steep, banana-shaped valley, with minimum value of 0 at (1,1). A starting point of (-1.2,1.0) was specified so that the initial gradient direction follows the curve of the valley.

$$F(x_1, x_2) = 100\left(x_2 - x_1^2\right)^2 + \left(1 - x_1\right)^2 \tag{E.1}$$

Least-squares form,

$$F(x_1, x_2) = \sum_{i=1}^{2} f_i^2 \tag{E.2}$$

$$f_1 = 10\left(x_2 - x_1^2\right)$$

$$f_2 = 1 - x_1$$

II. Helix Function

This function has a descending helical valley, with minimum value of 0 at (1,0,0). The starting point for the optimization was (-1,0,0).

$$F(x_1, x_2, x_3) = 100\left(\left(x_3 - 10\theta\right)^2 + (r-1)^2\right) + x_3^2 \tag{E.3}$$

$$r = \left(x_1^2 + x_2^2\right)^{1/2}$$

$$2\pi\theta = \tan^{-1}\left(\frac{x_2}{x_1}\right) \qquad , x_1 > 0$$

$$2\pi\theta = \pi + \tan^{-1}\left(\frac{x_2}{x_1}\right) \qquad , x_1 < 0$$

Least-squares form,

$$F(x_1, x_2, x_3) = \sum_{i=1}^{3} f_i^2 \tag{E.4}$$

$$f_1 = 10(x_3 - 100)$$

$$f_2 = 10(r - 1)$$

$$f_3 = x_3$$

III. Woods Function

This function has a near stationary point, which produces a variety of possible paths to a strong local minimum, at $F(x_i) \tilde{} 7.82$. The function has a global minimum value of 0 at (1,1,1,1). The starting point for the optimization was (-3,-1,-3,-1).

$$\begin{aligned} F(x_1, x_2, x_3, x_4) = {} & 100(x_2 - x_1^2)^2 + (1 - x_1)^2 + 90(x_4 - x_3^2)^2 \\ & + (1 - x_3)^2 + 10.1\{(x_2 - 1)^2 + (x_4 - 1)^2\} \\ & + 19.8(x_2 - 1)^2 \end{aligned} \tag{E.5}$$

Least-squares form,

$$F(x_1, x_2, x_3, x_4) = \sum_{i=1}^{6} f_i^2 \tag{E.6}$$

$$f_1 = 10\left(x_2 - x_1^2\right)$$

$$f_2 = 1 - x_1$$

$$f_3 = \sqrt{90}\left(x_4 - x_3^2\right)$$

$$f_4 = 1 - x_3$$

$$f_5 = \sqrt{29.9}\left(x_2 - 1\right)$$

$$f_6 = \sqrt{10.1}\left(x_4 - 1\right)$$

IV. Singular Function

This function is slowly varying in the neighborhood of the solution with minimum value of 0 at (0,0,0,0). The Hessian matrix is singular with two zero eigenvalues at the minimum. The starting point for the optimization was (-3,-1,0,-1).

$$F(x_1, x_2, x_3, x_4) = \left(x_1 + 10x_2\right)^2 + 5\left(x_3 - x_4\right)^2 + \left(x_2 - 2x_3\right)^4 + 10\left(x_1 - x_4\right)^4 \tag{E.7}$$

Least-squares form,

$$F(x_1, x_2, x_3, x_4) = \sum_{i=1}^{4} f_i^2 \tag{E.8}$$

$$f_1 = x_1 + 10x_2$$

$$f_2 = \sqrt{5}(x_3 - x_4)$$

$$f_3 = (x_2 - 2x_3)^2$$

$$f_4 = \sqrt{10}(x_1 - x_4)^2$$

V. Biggs Function

This function has a global minimum of 0 at (1,10,1,5,4) with a strong local minimum of 0.00265 near (1.78,16.12,-0.59,4.71,1.78). Since Eq. (E.9) is unchanged by interchanging x_1 with x_2 and interchanging x_3 with $-x_4$, a global minimum must also exist at (10,1,-5,-1,4). The starting point for the optimization was (1,2,1,1,1).

$$F(x_1, x_2, x_3, x_4, x_5) = \sum_{i=1}^{11} (x_3 e^{-x_1 z_i} - x_4 e^{-x_2 z_i} + 3e^{-x_5 z_i} - y_i)^2 \tag{E.9}$$

$$y_i = e^{-z_i} - 5e^{-10 z_i} + 3e^{-4 z_i}$$

$$z_i = 0.1i \qquad , i = 1, 2, \ldots, 11$$

Least-squares form,

$$F(x_1, x_2, x_3, x_4, x_5) = \sum_{i=1}^{11} f_i^2 \tag{E.10}$$

$$f_i = x_3 e^{-x_1 z_i} - x_4 e^{-x_2 z_i} + 3e^{-x_5 z_i} - y_i$$

VI. Polynomial #1

This function has a minimum value of 0 at (0,0,0). The starting point for the optimization was (0.4,0.6,0.8).

$$F(x_1,x_2,x_3)=x_1^4+x_2^4+x_3^4 \tag{E.11}$$

Least-squares form,

$$F(x_1,x_2,x_3)=\sum_{i=1}^{3} f_i^2 \tag{E.12}$$

$$f_1=x_1^2$$

$$f_2=x_2^2$$

$$f_3=x_3^2$$

VII. Polynomial #2

This function has a minimum value of -5.8979 at (-1.4134,-1.8786,0.7070). The starting point for the optimization was (-1,-2,-3).

$$F(x_1,x_2,x_3)=x_1^4+x_2^4+x_3^4+3x_1x_2^2+x_2^3+x_1x_3 \tag{E.13}$$

Least-squares form,

$$4F(x_1,x_2,x_3)+\frac{185}{2}=\sum_{i=1}^{6} f_i^2 \tag{E.14}$$

$$f_1=x_2^2+6x_1$$

$$f_2 = x_2^2 + 2x_2$$

$$f_3 = \sqrt{2}(x_1 + x_3)$$

$$f_4 = 2\left(x_1^2 - \frac{19}{4}\right)$$

$$f_5 = \sqrt{2}(x_2^2 - 1)$$

$$f_6 = 2\left(x_3^2 - \frac{1}{4}\right)$$

VIII. Polynomial #3

This function has a minimum value of 0 at (0,0,0). The starting point for the optimization was (-1,-2,-3).

$$F(x_1, x_2, x_3) = (x_1 - x_2)^4 + (x_2 - x_3)^4 + x_1^2 \tag{E.15}$$

Least-squares form,

$$F(x_1, x_2, x_3) = \sum_{i=1}^{3} f_i^2 \tag{E.16}$$

$$f_1 = (x_1 - x_2)^2$$

$$f_2 = (x_2 - x_3)^2$$

$$f_3 = x_1$$

IX. Polynomial #4

This function has a minimum value of 0 at (0,0,0,0). The starting point for the optimization was (-1,-2,-3,-4).

$$F(x_1, x_2, x_3, x_4) = (x_1 - x_2 - x_3 - x_4)^4 + (2x_1 + 4x_3)^4 + (x_2 - x_3)^4 + (x_4 - x_1)^2 \tag{E.17}$$

Least-squares form,

$$F(x_1, x_2, x_3, x_4) = \sum_{i=1}^{4} f_i^2 \tag{E.18}$$

$$f_1 = (x_1 - x_2 - x_3 - x_4)^2$$

$$f_2 = (2x_1 + 4x_3)^2$$

$$f_3 = (x_2 - x_3)^2$$

$$f_4 = x_4 - x_1$$

X. Polynomial #5

This function has a minimum value of 0 at (0,0,0,0). The starting point for the optimization was (-1,-2,-3,-4).

$$F(x_1, x_2, x_3, x_4) = (x_1 - x_2 - x_3 - x_4)^4 + (2x_1 + 4x_3)^4 + 20(x_2 - x_3)^4 + (x_4 - x_1)^2 \tag{E.19}$$

Least-squares form,

$$F(x_1, x_2, x_3, x_4) = \sum_{i=1}^{4} f_i^2 \tag{E.20}$$

$$f_1 = (x_1 - x_2 - x_3 - x_4)^2$$

$$f_2 = (2x_1 + 4x_3)^2$$

$$f_3 = \sqrt{20}(x_2 - x_3)^2$$

$$f_4 = x_4 - x_1$$

VITA

David Howard Huddleston was born in Lebanon, Tennessee on September 11, 1955. He was graduated from Watertown High School in May 1973. The following September he entered Tennessee Technological University, and in June 1977 he received a Bachelor of Science degree in Engineering Science. He then entered graduate school at Virginia Polytechnic Institute and State University where he received his Master of Science degree in Engineering Science and Mechanics in December 1978. He was employed by TRW, Inc. in October 1978, changed employment to Pan Am World Services, Inc. in October 1981, and changed employment to Sverdrup Technology, Inc. in August 1983.

Mr. Huddleston was married on July 23, 1977 to Julia Christine VanZant of Lebanon, Tennessee. They are the proud parents of two children, Matthew Howard and Nathan Everette Huddleston.